J Immunol 168: 1001-1008, 2002

15) Luther SA, Bidgol A, Hargreaves DC, et al. Differing activities of homeostatic chemokines CCL19, CCL21, and CXCL12 in lymphocyte and dendritic cell recruitment and lymphoid neogenesis. J Immunol 169: 424-433, 2002

16) Drayton DL, Ying X, Lee J, Lesslauer W, and Ruddle NH. Ectopic LTab directs lymphoid organ neogenesis with concomitant expression of peripheral node addressin and a HEV-restricted sulfotransferase. J Exp Med 197: 1153-1163, 2003

17) Drayton DL, Liao S, Mounzer RH, Ruddle NH. Lymphoid organ development: from ontogeny to neogenesis. Nat Immunol 7:344-353, 2006

18) Endres R, Alimzhanov MB, Plitz T, et al. Mature follicular dendritic cell networks depend on expression of lymphotoxin b receptor by radioresistant stromal cells and of lymphotoxin b and tumor necrosis factor by B cells. J Exp Med 189: 159-168, 1999

19) Ngo VN, Korner H, Gunn MD, et al. Lymphotoxin a/b and tumor necrosis factor are required for stromal cell expression of homing chemokines in B and T cell areas of the spleen. J Exp Med 189: 403-412, 1999

20) Bajéoff M, Egen JG, Qi H, Huang AY, Castellino F, Germain RN. Highways, byways and breadcrumbs: directing lymphocyte traffic in the lymph node. Trends Immunol 28:346-352, 2007

21) Nakashima M, Mori K, Maeda K, et al. Selective elimination of double-positive immature thymocytes by a thymic epithelial cell line. Eur J Immunol 20: 47-53, 1990

22) Schrama D, thor Straten P, Fischer WH, et al. Targeting of lymphotoxin-a to the tumor elicits an efficient immune response associated with induction of peripheral lymphoid-like tissue. Immunity 14: 111-121, 2001

23) Suematsu S and Watanabe T. Generation of a synthetic lymphoid tissue-like organoid in mice. Nat Biotech 22: 1539-1545, 2004

24) Okamoto N, Chihara R, Shimizu C, Nishimoto S, Watanabe T. Artificial lymph nodes induce potent secondary immune responses in naive and immunodeficient mice. J Clin Invest 117:997-1007, 2007

THE JOURNAL OF BIOLOGICAL CHEMISTRY VOL. 283, NO. 2, pp. 998–1007, January 11, 2008


# Creation and X-ray Structure Analysis of the Tumor Necrosis Factor Receptor-1-selective Mutant of a Tumor Necrosis Factor-$\alpha$ Antagonist*

Received for publication, September 21, 2007, and in revised form, November 2, 2007 Published, JBC Papers in Press, November 14, 2007, DOI 10.1074/jbc.M707933200

**Hiroko Shibata,[a,b] Yasuo Yoshioka,[a,c] Akiko Ohkawa,[a] Kyoko Minowa,[a,d] Yohei Mukai,[a,e] Yasuhiro Abe,[a,e] Madoka Taniai,[f] Tetsuya Nomura,[a,e] Hiroyuki Kayamuro,[a,e] Hiromi Nabeshi,[a,e] Toshiki Sugita,[a,e] Sunao Imai,[a,e] Kazuya Nagano,[a,e] Tomoaki Yoshikawa,[a] Takuya Fujita,[d] Shinsaku Nakagawa,[c,e] Akira Yamamoto,[d] Tsunetaka Ohta,[f] Takao Hayakawa,[b] Tadanori Mayumi,[g] Peter Vandenabeele,[h] Bharat B. Aggarwal,[i] Teruya Nakamura,[j] Yuriko Yamagata,[j] Shin-ichi Tsunoda,[a,c] Haruhiko Kamada,[a,c1] and Yasuo Tsutsumi[a,c,e]**

*From the [a]National Institute of Biomedical Innovation, 7-6-8 Saito-Asagi, Ibaraki, Osaka 567-0085, Japan, [b]National Institute of Health Science, 1-18-1 Kamiyoga, Setagaya-ku, Tokyo 158-8501, Japan, [c]Center for Advanced Medical Engineering and Informatics, Osaka University, 1-6 Yamadaoka, Suita, Osaka 565-0871, Japan, [d]Kyoto Pharmaceutical University, Misasagi-Nakauchicho 5, Yamashina-ku, Kyoto 607-8414, Japan, [e]Graduate School of Pharmaceutical Sciences, Osaka University, 1-6 Yamadaoka, Suita, Osaka 565-0871, Japan, [f]Hayashibara Biochemical Laboratories, Inc., 1-2-3 Shimoishii, Okayama 702-8006, Japan, [g]Graduate School of Pharmaceutical Sciences, Kobe Gakuin University, 518 Arise, Igawadani, Nishi-ku, Kobe 651-2180, Japan, the [h]Department of Molecular Biomedical Research, Flanders Institute for Biotechnology and the Department of Molecular Biology, Ghent University, B-9052 Ghent, Belgium, the [i]Department of Experimental Therapeutics, University of Texas M. D. Anderson Cancer Center, Houston, Texas 77030, and [j]Faculty of Medical and Pharmaceutical Sciences, Kumamoto University, 5-1 Ooehonmachi, Kumamoto 862-0973, Japan*

Tumor necrosis factor-$\alpha$ (TNF) induces inflammatory response predominantly through the TNF receptor-1 (TNFR1). Thus, blocking the binding of TNF to TNFR1 is an important strategy for the treatment of many inflammatory diseases, such as hepatitis and rheumatoid arthritis. In this study, we identified a TNFR1-selective antagonistic mutant TNF from a phage library displaying structural human TNF variants in which each one of the six amino acid residues at the receptor-binding site (amino acids at positions 84–89) was replaced with other amino acids. Consequently, a TNFR1-selective antagonistic mutant TNF (R1antTNF), containing mutations A84S, V85T, S86T, Y87H, Q88N, and T89Q, was isolated from the library. The R1antTNF did not activate TNFR1-mediated responses, although its affinity for the TNFR1 was almost similar to that of the human wild-type TNF (wtTNF). Additionally, the R1antTNF neutralized the TNFR1-mediated bioactivity of wtTNF without influencing its TNFR2-mediated bioactivity and inhibited hepatic injury in an experimental hepatitis model. To understand the mechanism underlying the antagonistic activity of R1antTNF, we analyzed this mutant using the surface plasmon resonance spectroscopy and x-ray crystallography. Kinetic association/dissociation parameters of the R1antTNF were higher than those of the wtTNF, indicating very fast bond dissociation. Furthermore, x-ray crystallographic analysis of R1antTNF suggested that the mutation Y87H changed the binding mode from the hydrophobic to the electrostatic interaction, which may be one of the reasons why R1antTNF behaved as an antagonist. Our studies demonstrate the feasibility of generating TNF receptor subtype-specific antagonist by extensive substitution of amino acids of the wild-type ligand protein.

Tumor necrosis factor (TNF)[2] is a major inflammatory cytokine that, like the other members of the TNF superfamily of ligands, plays a central role in host defense and inflammation (1). Elevated serum levels of TNF correlate with the severity and progression of the inflammatory diseases such as rheumatoid arthritis, inflammatory bowel disease, septic shock, multiple sclerosis, and hepatitis (2–4). So far, anti-TNF antibodies and soluble TNFRs, which interfere with the activity of TNF, have been used to treat various inflammatory diseases (5, 6). However, these therapies can cause serious side effects, such as bacterial and virus infection, lymphoma development, and lupus inflammatory disease (7–10), because they also inhibit the TNF-

* This work was supported in part by Grants-in-aid for Scientific Research 18015055, 18659047, and 7689008 from the Ministry of Education, Culture, Sports, Science and Technology of Japan and Japan Society for the Promotion of Science, by a Health Labor Sciences research grant from the Ministry of Health, Labor and Welfare of Japan, by Health Sciences research grants for research on health sciences focusing on drug innovation from the Japan Health Sciences Foundation, and in part by Japan Society for the Promotion of Science Research Fellowships for Young Scientists 02872, 08841, 09131. The costs of publication of this article were defrayed in part by the payment of page charges. This article must therefore be hereby marked "*advertisement*" in accordance with 18 U.S.C. Section 1734 solely to indicate this fact.

*The atomic coordinates and structure factors (code 2E7A) have been deposited in the Protein Data Bank, Research Collaboratory for Structural Bioinformatics, Rutgers University, New Brunswick, NJ (http://www.rcsb.org/).*

[1] To whom correspondence should be addressed: Laboratory of Pharmaceutical Proteomics, National Institute of Biomedical Innovation, 7-6-8 Saito-Asagi, Ibaraki, Osaka 567-0085, Japan. Fax: 81-72-641-9817; E-mail: kamada@nibio.go.jp.

[2] The abbreviations used are: TNF, tumor necrosis factor $\alpha$; TNFR, TNF receptor; PDB, Protein Data Bank; PBS, phosphate-buffered saline; RT, reverse transcription; HUVEC, human umbilical vein endothelial cells; ELISA, enzyme-linked immunosorbent assay; GM-CSF, granulocyte-macrophage colony-stimulating factor; TES, 2-([2-hydroxy-1,1-bis(hydroxymethyl)ethyl]amino)ethanesulfonic acid; EAE, experimental autoimmune encephalomyelitis; ALT, alanine aminotransferase; h, human; m, mouse; mut, mutant.

dependent host defense function of the patients. TNF blockade by administering these agents into patients with multiple sclerosis was also shown to aggravate their symptoms (11). Therefore, to overcome these problems, development of a new therapeutic strategy is highly desirable.

TNF binds to two receptor subtypes, p55 TNF receptor (TNFR1) and p75 TNF receptor (TNFR2), to exert its biological functions (12). Thus, functional analyses of the TNF receptors were carried out to explore a new therapeutic strategy. Previous studies using animal models of diseases such as arthritis and hepatitis demonstrated the predominant role of TNFR1 in the pathogenesis and exacerbation of inflammation (13, 14). In the experimental autoimmune encephalomyelitis model (EAE), which is widely used as an animal model of multiple sclerosis, the symptoms exacerbated significantly in the TNF knock-out mice compared with that in the wild-type mice (15). Another study indicates that the TNF has a dual role on the EAE model, an inflammatory and immunosuppressive effect, and although the immunosuppressive effect does not require the TNFR1, it is essential for the acute phase inflammation of EAE (16). On the other hand, although the TNFR1 is believed to be important for the defense mechanism against mycobacterium, the membrane-bound TNF, the prime activating ligand of TNFR2, was reported to be sufficient to control the mycobacterial infection (17, 18). Moreover, TNFR2 was shown to be crucial for the proliferation, activation, and antigen presentation of the T-cells, which are essential in the cell-mediated immune response against bacteria and virus (19–21). Therefore, blocking the TNFR1-mediated signal transduction emerged as a potential therapeutic strategy with low side effects for the inflammatory diseases.

From these perspectives, attempts were made to develop drugs targeted to TNFR1. Along with the progress of antibody engineering, attempts were made to develop an anti-TNFR1 antibody with antagonistic activity. But the desired antibody could not be created, because the anti-TNFR1 antibodies recognizing the TNF-binding site on TNFR1 acted like a TNFR1 agonist and not an antagonist (22). Attempts to design a low molecular weight TNFR1 antagonist based on the three-dimensional structural information of the TNFR1 was also not successful in identifying an antagonist that would selectively inhibit the TNF/TNFR1 interaction and would have sufficient therapeutic effect (23, 24). In this respect, we previously 1) constructed two phage libraries displaying the structural TNF variants in which six amino acid residues (amino acids 29, 31, 32, 145–147, library I; amino acids 84–89, library II) in the predicted receptor binding sites were replaced with other amino acid, 2) and we successfully identified the TNFR1-selective mutant with great biological activity from the library I.[3] In the screening process, mutants with high affinity for the TNFR1 and great TNFR1 selectivity were found from library II, although their biological activities were very weak.[3] The strategy described here could comprehensively assess the affinities and bioactivities of TNF variants, thus enabling the high-throughput screening of TNFR1-selective antagonists, which have no biological activity but high TNFR1 affinity. In this study, we analyzed the biological activity and TNFR1 affinity of 500 TNF variants, which were concentrated by panning against the TNFR1, and we subsequently isolated a novel TNFR1-selective antagonistic mutant TNF (R1antTNF). R1antTNF showed exclusive TNFR1 selectivity, and it efficiently inhibited wide varieties of TNFR1-mediated effects of the wild-type TNF *in vitro* and *in vivo*. Additionally, we used surface plasmon resonance and x-ray structural analyses to elucidate the underlying cause for the antagonist activity of R1antTNF.

## EXPERIMENTAL PROCEDURES

*Cell Culture*—L-M cells (a mouse fibroblast cell line) were provided by Mochida Pharmaceutical Co. Ltd. (Tokyo, Japan) and were maintained in minimum Eagle's medium (Sigma) supplemented with 1% fetal bovine serum and 1% antibiotic mixture (penicillin 10,000 units/ml, streptomycin 10 mg/ml, and amphotericin B 25 μg/ml) (Nacalai Tesque, Kyoto, Japan). HEp-2 cells (a human fibroblast cell line) were provided by Cell Resource Center for Biomedical Research (Tohoku University, Sendai, Japan) and were maintained in RPMI 1640 medium (Sigma) supplemented with 10% fetal bovine serum and 1% antibiotic mixture (Nacalai Tesque). PC60-R1 and PC60-R2 cells (a mouse-rat fusion hybridoma consisting of human TNFR1- or TNFR2-transfected PC60 cells) were established as described previously (25) and maintained in RPMI 1640 medium supplemented with 10% fetal bovine serum, 1 mM sodium pyruvate, $5 \times 10^{-5}$ M 2-mercaptoethanol, 3 μg/ml puromycin (Wako Pure Chemical Industries, Osaka, Japan), and 1% antibiotic mixture.

*Cytokines, Receptors, and Antibodies*—Recombinant human TNFR1 or TNFR2 Fc chimera, biotinylated anti-human TNF polyclonal antibody, and horseradish peroxidase-conjugated horseradish peroxidase were purchased from R & D Systems (Minneapolis, MN). Recombinant human or mouse TNF and IL-1β were purchased from PeproTech (Rocky Hill, NJ). The recombinant human TNF used for the *in vivo* hepatitis examination and the recombinant wtTNF-FLAG (a FLAG tag fusion protein of human TNF) were purified in our laboratory. We confirmed that the bioactivity of each TNF was equal to that of commercially available recombinant human TNF. Anti-FLAG M2 antibody was purchased from Sigma. Goat anti-human IgG antibody was purchased from Cappel (West Chester, PA). Anti-human Fas IgM was purchased from MBL (Nagoya, Japan).

*Selection of Phage Displaying Structural TNF Variants (Panning)*—Human TNFR1 Fc chimera was diluted to 50 μg/ml in 10 mM sodium acetate buffer, pH 4.5, and immobilized to a CM3 sensor chip using an amine coupling kit (BIAcore®, Uppsala, Sweden), which resulted in an increase of 4,000–6,000 resonance units. The phage library ($1 \times 10^{11}$ colony-forming units/100 μl) was injected at the flow rate of 3 μl/min over the sensor chip. After injection, the sensor chip was washed using the rinse command. Elution was carried out using 20 μl of 10 mM glycine HCl. The eluted phages were neutralized with 1 M Tris-HCl, pH 6.9. *Escherichia coli* (TG1) was infected with the eluted phages for amplification. These steps were performed twice. After the second round of selection, the phage mixture was used to infect *E. coli* and plated on LB agar/ampicillin

[3] Y. Abe, H. Shibata, K. T. Nomura, K. Minowa, H. Kamada, S. Tsunoda, Y. Tsutsumi, unpublished data.

plates. Five hundred individual colonies of *E. coli* infected with phage clones were individually picked from the LB agar plates, and each colony was grown in 2-YT medium with ampicillin (100 μg/ml) and glucose (2% w/v) at 37 °C until the $A_{600}$ of the culture medium reached 0.4. Each culture was centrifuged; the supernatants were removed, and fresh 2-YT media with ampicillin (100 μg/ml) was added to each *E. coli* pellet. After incubation for 6 h at 37 °C, supernatants were collected and used to measure cytotoxicity in human HEp-2 cells (26, 27) and to determine the affinity for TNFR1 by ELISA (28). To measure cytotoxicity, HEp-2 cells were cultured in 96-well plates with 10% *E. coli* supernatant and 100 μg/ml cycloheximide for 18 h at $4 \times 10^4$ cells/well, and cytotoxicity was assessed by methylene blue assay as described previously (26). To determine the affinity for TNFR1 by ELISA, wells of the immune assay plates were first coated with the goat anti-human IgG antibody and then incubated with the recombinant human TNFR1 Fc chimera (0.2 μg/ml). After blocking, 2-fold diluted *E. coli* supernatant was added into each well, and the plates were incubated for 2 h at 37 °C. To each well, 200 ng/ml biotinylated anti-human TNF polyclonal antibody was added, and the plates were further incubated for 1 h at 37 °C. Wells were washed and then incubated with 1000-fold diluted avidin-horseradish peroxidase. Next, wells were washed; TMB peroxidase substrate (MOSS, Inc. Pasadena, MD) was added to each well, and the absorbance was read at 450/650 nm using a micro-plate reader.

*Expression and Purification of mutTNFs*—Protocol for the expression and purification of recombinant proteins was described previously (29). Briefly, mutTNFs were overexpressed in *E. coli* BL21(DE3). Expressed mutTNFs were recovered from the inclusion body, which were washed with 2.5% Triton X-100 and 0.5 M NaCl in TES buffer, and solubilized in 6 M guanidine HCl, 0.1 M Tris-HCl, pH 8.0, and 2 mM EDTA. The solubilized protein was reduced with 10 mg/ml dithioerythritol for 4 h at room temperature and then refolded by 100-fold dilution in a refolding buffer (100 mM Tris-HCl, 2 mM EDTA, 0.5 M arginine, and oxidized glutathione (551 mg/liter)). After dialyzing against 20 mM Tris-HCl, pH 7.4, containing 100 mM urea, the active trimeric proteins were purified by Q-Sepharose and Mono Q chromatography. An additional size-exclusion chromatography (Superose 12, GE Healthcare) was performed to further purify each protein. Endotoxin levels in the purified mutTNF were determined to be <300 pg/mg.

*Cytotoxicity Assay*—For the cytotoxicity assay, mouse L-M cells were cultured in the 96-well plates ($1 \times 10^4$ cells/well) in the presence of serially diluted mouse wtTNF or mutTNFs. For the neutralization assay, cells were cultured in the presence of a constant concentration of the mouse wtTNF (5 ng/ml) and a serial dilution of the mutTNF. After incubation for 48 h, cell survival was determined by methylene blue assay as described previously (26). Jurkat cells were incubated in 96-well plates ($1 \times 10^4$ cells/well) with 0.2 ng/ml anti-human Fas IgM and serially diluted R1antTNF for 24 h, and cytotoxicity was assessed using the 3-(4,5-dimethylthiazol-2-yl)-2,5-diphenyltetrazolium bromide assay.

*Competitive ELISA*—Inhibition of wtTNF binding to the hTNFR1 and hTNFR2 by R1antTNF was measured by ELISA as reported previously (28). The wtTNF-FLAG, a FLAG tag fusion protein of human TNF, was used as a marker protein. Briefly, the immune assay plates were coated with the goat anti-human IgG antibody and incubated with either the human TNFR1 or the human TNFR2 (0.2 μg/ml). After blocking, premixed wtTNF-FLAG (100 ng/ml) and various concentrations of R1antTNF were added to the plates. After 2 h of incubation at room temperature, the wells were washed, and the biotinylated anti-FLAG M2 antibody (0.5 μg/ml) was added to each well and then incubated for an additional period of 2 h at room temperature. Wells were washed and then incubated with the horseradish peroxidase-coupled streptavidin for 30 min at room temperature. The remaining bound wtTNF-FLAG was quantified as described above.

*PC60 Assay*—PC60-R1 and PC60-R2 cells were cultured at $5 \times 10^4$ cells/well with IL-1β (2 ng/ml). To evaluate the inhibitory activity, serially diluted R1antTNF and human wtTNF (200 ng/ml for PC60-R1 and 40 ng/ml for PC60-R2) were added to each cell type. After 24 h of incubation, the amount of rat GM-CSF produced was quantified by ELISA according to the manufacturer's protocol (R & D Systems).

*Caspase-3/7 and NF-κB Activities*—To measure the caspase-3/7 activity, the L-M cells were incubated with the human wtTNF (60 ng/ml) and R1antTNF for 8 h, and then an equal volume of the Caspase-Glo 3/7 Assay reagent (Promega Japan, Tokyo, Japan) was added to the cells. The cells were further incubated for 1 h, and luminescence was then measured using a plate reader (ALVO series, PerkinElmer Life Sciences). To measure the NF-κB activity, nuclear proteins were collected from the L-M cells stimulated with the human wtTNF (5 ng/ml) and R1antTNF for 1 h, and the activity of the NF-κB p65 in the treated cells was determined using the TransAM NF-κB p65 kit (Active Motif, Carlsbad, CA). Nuclear protein extract (1 μg) was added to an oligonucleotide-coated plate and was visualized using an anti-NF-κB p65 antibody.

*RT-PCR Analysis*—Total RNA was extracted from the human wtTNF and R1antTNF-stimulated HUVEC using an RNeasy mini kit (Qiagen, Valencia, CA). First-strand cDNA was synthesized from 1 μg of total RNA by using an oligo($dT_{12-18}$) primer and SuperScript III reverse transcriptase (Invitrogen). Real time quantitative RT-PCR was performed using the TaqMan assay, and the PCR amplifications were carried out using an ABI 7000 thermocycler (Applied Biosystems, Foster City, CA). cDNA samples were added into a PCR master mix containing the Platinum qPCR super mix (Invitrogen) and primer/fluorescent probe sets (TaqMan Gene Expression Assays, Applied Biosystems) for the human β-actin, E-selectin, and ICAM-1 in 96-well PCR plates. Conditions for PCR were 2 min at 50 °C, 2 min at 95 °C, 45 cycles of denaturation at 95 °C for 15 s, and annealing/extension step at 60 °C for 5 s. The threshold cycle (*CT*) during the exponential phase of amplification was determined using the ABI Prism® 7000 SDS software.

*Induction of Lethal Hepatitis*—BALB/c mice (6-week-old females) were purchased from CLEA Japan (Tokyo, Japan). All experimental protocols for animal studies were in accordance with "Principles of Laboratory Animal Care" (National Institutes of Health) and our institutional guidelines. All reagents were prepared in pyrogen-free PBS. Control mice were injected

intravenously with 200 μl of the mixture, 100 μl of PBS, 50 μl of 20 μg/ml wtTNF, and 50 μl of 400 mg/ml GalN. Experimental mice were injected intravenously with 200 μl of the mixture, 100 μl of R1antTNF (2.7, 0.3, or 0.1 mg/ml), 50 μl of 20 μg/ml wtTNF, and 50 μl of 400 mg/ml GalN. In preliminary experiments, serum ALT levels began to increase at 6 h and were maximal 9 h after the administration of TNF/GalN. The dose used was lethal in 80–100% of mice. Blood samples were obtained from the orbital plexus under light ether anesthesia 9 h after the challenge. The serum ALT concentration was measured using a colorimetric assay kit from Wako Pure Chemical (Osaka, Japan).

*Surface Plasmon Resonance Assay (BIAcore® Assay)*—The binding kinetics of the wtTNF and R1antTNF were analyzed by the surface plasmon resonance (BIAcore®) technique. TNFRs were immobilized onto a CM5 sensor chip, which resulted in an increase of 3,000–3,500 resonance units. During the association phase, R1antTNF or wtTNF, diluted in running buffer (HBS-EP) at 26.1 nM, 8.7 nM or 2.9 nM, was allowed to pass over the immobilized TNFRs at a flow rate of 20 μl/min. During the dissociation phase, HBS-EP buffer was applied to the sensor chip at a flow rate of 20 μl/min. The data were analyzed globally with the BIAevaluation 3.0 software (BIAcore®) using a 1:1 binding model.

*X-ray Crystallography*—Purified R1antTNF was concentrated to 10 mg/ml in 20 mM Tris-HCl, pH 7.4. Initial screening using Hampton Crystal screen 1, 2 and Index kit was performed by the vapor-diffusion method with hanging drops (1 + 1 μl) at 20 °C. After optimization of crystallization conditions, orthorhombic crystals ($0.2 \times 0.2 \times 0.4$ mm$^3$) were obtained with 0.05 M HEPES, pH 7.5, 1.5% w/v 1,2,3-heptanetriol, and 12.5% PEG 3350. Crystals were frozen in a reservoir solution containing 20% glycerol as a cryoprotectant. X-ray diffraction data to 1.8 Å resolution were collected at the BL41XU, SPring-8 synchrotron, Harima, Japan, under flash-cooling to 100 K to reduce the effects of radiation damage. Data reduction was carried out using the DENZO and SCALEPACK. Molecular replacement was performed by using the Molrep program in ccp4i (30) using a crystal structure of the wtTNF (1TNF) (31) as a model. Cycles of manual rebuilding using O (32) and refinement using CNS (33) led to a refined structure. Final model validation was performed using the Procheck program in ccp4i (30). The model complexes of TNF-TNFR1 and R1antTNF-TNFR1 were constructed based on the crystal structure of the LT-α-TNFR1 complex (31) by using the superpose program in ccp4i.

## RESULTS

*Selection of TNFR1-selective mutTNF Antagonists*—We previously constructed a phage library that displays structural variants of the human TNF in which random amino acid sequences replace the 6 residues (amino acids 84–89) that have been predicted to be in the TNF receptor-binding site from the crystal structure of the LT-α-TNFR1 complex (31). We confirmed that the phage library consisted of $1 \times 10^7$ independent recombinant clones. To isolate a TNFR1-selective mutant TNF (mutTNF) antagonist, the phage library was subjected to two rounds of panning against the human TNFR1 (hTNFR1) using the BIAcore® biosensor, and recovered clones were assessed for

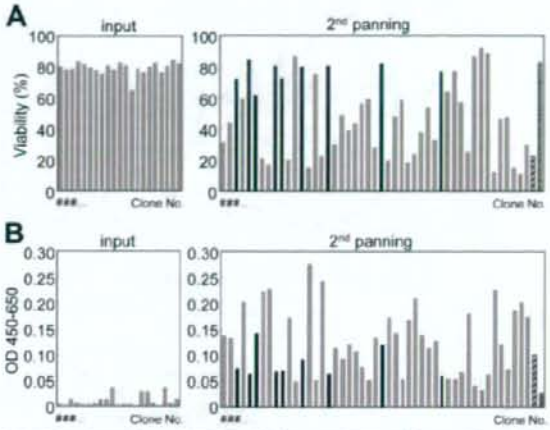


FIGURE 1. **Screening of TNFR-selective mutTNFs with no bioactivity.** Selected phage clones from the phage library were used to infect *E. coli* in a 96-well plate, and the supernatant from each infected *E. coli* was assessed to determine the bioactivity (*A*) and binding affinity (*B*) of each mutTNF. *A*, Hep-2 cells were incubated with the *E. coli* supernatant for 18 h, and cell viability was measured using the methylene blue assay. *B*, each *E. coli* supernatant was applied to the TNFR1-immobilized plate, and binding of the mutTNF to the TNFR1 was detected using the biotinylated polyclonal anti-TNF antibody. ■, mutTNF clones binding specifically to TNFR1; ▨, wtTNF; ▤, negative control.

**TABLE 1**

**Nucleotide and amino acid sequences of 10 candidate TNFR1-selective mutTNF antagonists, which had high affinity for TNFR1 and no TNFR1 bioactivity**

| Clone | Position | | | | | |
|---|---|---|---|---|---|---|
| | Ala-84 | Val-85 | Ser-86 | Tyr-87 | Gln-88 | Thr-89 |
| T1 | G(GGC) | H(CAC) | L(TCC) | Y(TAC) | T(ACG) | T(AAC) |
| T2 | S(AGC) | T(ACC) | T(ACC) | H(CAC) | N(AAC) | Q(CAG) |
| T3 | T(ACC) | S(AGC) | V(GTC) | Y(TAC) | P(CCC) | H(CAC) |
| T4 | T(ACC) | N(AAC) | I(ATC) | Y(TAC) | S(AGC) | N(AAC) |
| T5 | N(AAC) | G(GGC) | A(GCG) | Y(TAC) | E(GAG) | T(ACG) |
| T6 | G(GGC) | G(GGC) | P(CCG) | Y(TAC) | Q(CAG) | R(CGG) |
| T7 | S(AGC) | P(CCG) | R(AGG) | V(GTC) | S(TCC) | G(GGC) |
| T8 | T(ACC) | P(CCC) | A(GCC) | I(ATC) | N(AAC) | R(CGG) |
| T9 | A(GCG) | P(CCC) | G(GGC) | Y(TAC) | S(TCC) | H(CAC) |
| T10 | S(TCC) | P(CCC) | Q(CAG) | Y(TAC) | S(AGC) | V(GTC) |

TNFR1-mediated cytotoxicity and affinity for TNFR1. Although the number of phage clones that had strong cytotoxicity increased after the second panning, phage clones having almost no cytotoxicity but significant affinity for TNFR1 were also recognized (Fig. 1). Eventually, we identified 10 mutTNF candidates as the TNFR1-selective antagonists (Table 1), and we further investigated the properties of these 10 potential antagonists. All 10 mutTNFs were recombinantly expressed in *E. coli*, out of which we could only purify nine mutTNFs (T1–T4, T6–T10); for some unknown reason, we were unable to purify the mutTNF-T5. All nine purified mutTNFs displayed a molecular mass of 17 kDa by gel electrophoresis and gel filtration analyses and formed homotrimeric complexes in the same manner as the wtTNF (data not shown). We measured the bioactivities and antagonistic activities of nine mutTNFs on the mouse TNFR1 (mTNFR1) using the L-M cells, a cell line derived from the L929 cells, and the results are shown in Fig. 2. The mutTNF-T2 showed the lowest biological activity even when tested at high concentrations (Fig. 2*A*). Both mutTNF-T2 and mutTNF-T7 inhibited the wtTNF-induced cytotoxicity

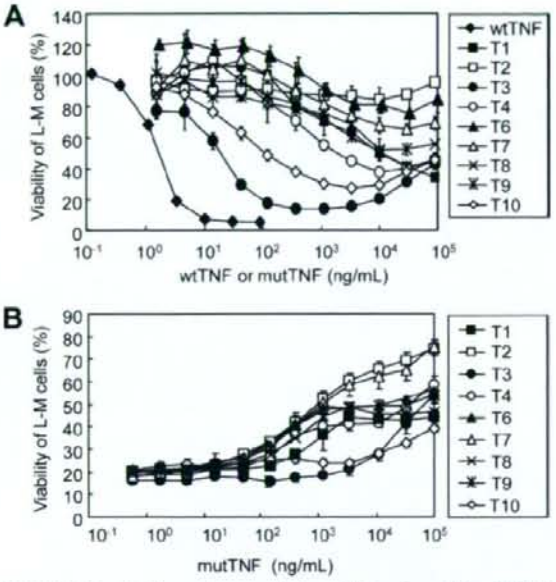


FIGURE 2. **Bioactivities and antagonistic activities of candidate TNFR1-selective mutTNFs.** *A*, diluted mutTNFs were added to the L-M cells and incubated for 48 h at 37 °C. After incubation, cell viability was measured using the methylene blue assay. *B*, indicated dilutions of a given mutTNF and a constant concentration of mouse TNF (5 ng/ml) were mixed and added to the L-M cells. Cell viability was measured as described above, and the antagonistic activity was assessed as described under "Experimental Procedures." Each data point represents the mean ± S.D.

**TABLE 2**

**Dissociation constants of the mutTNFs determined from the SPR analysis of the interactions between the mutTNFs and the hTNFR1 or hTNFR2**

| Clone | TNFR1 $K_D$ | TNFR2 $K_D$ | TNFR1 selectivity |
|---|---|---|---|
| | nM | nM | |
| wtTNF | 1.4 | 2.1 | 1.0 |
| T1 | 5.0 | 28.1 | 3.7 |
| T2 | 3.5 | 92,900.0 | 17,677.4 |
| T3 | 1.2 | 4.6 | 2.6 |
| T4 | 5.0 | 26.9 | 3.5 |
| T6 | 7.6 | 2.3 | 0.2 |
| T7 | 2.3 | 12.9 | 3.7 |
| T8 | 2.6 | 1230.0 | 308.8 |
| T9 | 6.8 | 8.4 | 0.8 |
| T10 | 5.1 | 8.8 | 1.1 |

most efficiently (Fig. 2*B*). Additionally, the TNF receptor selectivity of the nine mutants was measured using the BIAcore® biosensor technique. Both mutTNF-T2 and mutTNF-T8 showed superior TNFR1 selectivity as compared with the other mutants (Table 2). Based on these results, mutTNF-T2 was chosen for further analysis and renamed as R1antTNF; this mutant displayed the highest selectivity for TNFR1 binding and possessed the lowest biological activity and highest antagonistic activity on mTNFR1.

*Inhibition of TNFR1-mediated Intracellular Signaling and Expression of Adhesion Molecule by R1antTNF*—Activation of TNFR1 by TNF leads to the recruitment of the adaptor protein TRADD to its cytoplasmic death domain and induction of apoptosis because of the activation of caspase-8/10 and caspase-3/7 (34). If R1antTNF inhibited the wtTNF-mediated cytotoxicity

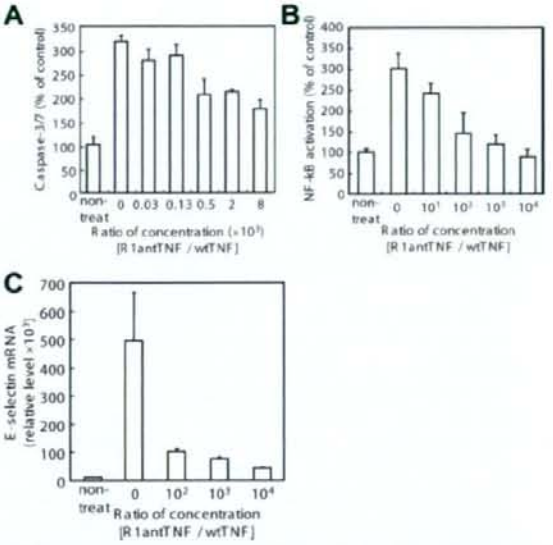


FIGURE 3. **R1antTNF-mediated inhibition of signal transduction and expression of adhesion molecule.** Activation of caspase-3/7 (*A*) and NF-κB (*B*) induced by the human wtTNF (60 and 5 ng/ml, respectively) in L-M cells was measured as described under "Experimental Procedures." Incubation times for the caspase-3/7 was 8 h and that for the NF-κB was 1 h. *C*, to measure the E-selectin expression, indicated amounts of R1antTNF were mixed with the human wtTNF (10 ng/ml), and the mixture was added to the HUVEC and incubated for 3 h. Total RNAs were prepared from these cells and were used for the RT-PCR analysis. Each data point represents the mean ± S.D.

in L-M cells by blocking the binding of wtTNF to TNFR1, R1antTNF could also inhibit this activation of caspase cascade. Thus, we investigated the inhibitory activity of R1antTNF on the wtTNF-induced activation of caspase-3/7. Indeed R1antTNF significantly inhibited the caspase-3/7 activation induced by the wtTNF in L-M cells in a dose-dependent manner (Fig. 3*A*). TNFR1 signaling also activates the transcription factor NF-κB, leading to the activation of inflammatory and anti-apoptotic genes (34). We found that the wtTNF-mediated NF-κB activation in mouse L-M cells was completely blocked by the addition of R1antTNF (Fig. 3*B*). NF-κB activated by the TNF/TNFR1 interaction regulates several cell adhesion molecules in the endothelial cells, such as E-selectin, ICAM-1, and VCAM-1 (35). Therefore, we assessed the inhibitory activity of R1antTNF on the wtTNF-induced expression of cell adhesion molecules in HUVEC cells. We found that the R1antTNF suppressed the expression of the E-selectin gene (Fig. 3*C*). These results suggested that R1antTNF inhibited the function of wtTNF by blocking the wtTNF-induced signal transduction.

*TNFR1-selective Antagonistic Activity of R1antTNF*—To determine the potency of the TNFR1-selective antagonistic activity, we used competitive ELISA to investigate whether the R1antTNF would inhibit only the binding of the wtTNF to hTNFR1. R1antTNF inhibited the binding of wtTNF to hTNFR1 in a dose-dependent manner just like the wtTNF did, but it did not affect the binding of wtTNF to hTNFR2 (Fig. 4, *A* and *B*). This result correlates to the results obtained using the BIAcore technique. To confirm that this antagonistic activity of R1antTNF was receptor-selective, a competitive bioassay was

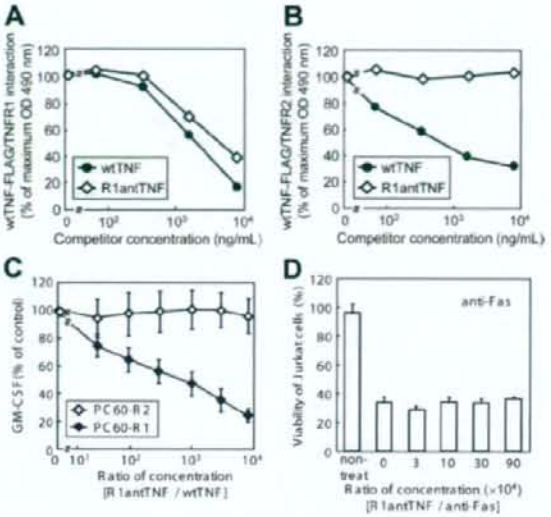


FIGURE 4. **TNFR1-selective antagonistic properties of R1antTNF.** Different concentrations of wtTNF and R1antTNF were premixed with a fixed concentration of wtTNF-FLAG and were added to the hTNFR1-coated (*A*) or hTNFR2-coated plates (*B*). Binding of wtTNF-FLAG was determined as described under "Experimental Procedures." *C*, to determine the receptor-type contribution to bioactivity, serially diluted R1antTNF was mixed with the human wtTNF (PC60-R1, 200 ng/ml; PC60-R2, 40 ng/ml), and added to the PC60-Rs cells. After 24 h, production of the rat GM-CSF was measured by ELISA as described under "Experimental Procedures." ◆, PC60-R1; 224 , PC60-R2. *D*, Jurkat cells were incubated with the anti-human Fas IgM (0.2 ng/ml) and indicated dilutions of R1antTNF for 24 h, and cytotoxicity was assessed using the 3-(4,5-dimethylthiazol-2-yl)-2,5-diphenyltetrazolium bromide assay.

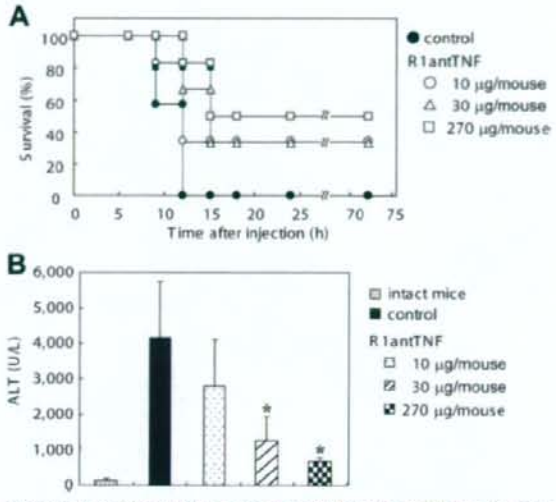


FIGURE 5. **Therapeutic effect of R1antTNF in lethal hepatitis model.** Mice were injected intravenously with recombinant human TNF (1.0 μg)/GalN (20 mg) and R1antTNF or PBS. *A*, survival rates of the mice in the TNF/GalN-induced hepatitis model were measured over a period of 72 h ($n = 6$). *B*, blood samples were collected 9 h after the challenge. Serum concentration of alanine aminotransferase (*ALT*) was measured as described under "Experimental Procedures" ($n = 6$). Data represent the mean ± S.E. Statistical significance *versus* control mice was calculated by unpaired Student's *t* test (*, $p < 0.05$).

performed using PC60-R1 and PC60-R2 cell lines that stably expressed hTNFR1 and hTNFR2 (25), respectively. R1antTNF efficiently inhibited the wtTNF-induced GM-CSF production in the PC60-R1 cells but not in the PC60-R2 cells (Fig. 4*C*), confirming the TNFR1-specific antagonistic activity. The risk of cross-activity to other TNF receptor superfamily members was assessed by Fas-induced cytotoxicity assay on Jurkat cell (Fig. 4*D*). R1antTNF did not affect the Fas-mediated signaling, which suggest that R1antTNF was highly selective proteo-antagonist of TNFR1. These data suggest that the R1antTNF not only binds to the TNFR1 selectively but also has TNFR1-selective inhibitory activity.

*Therapeutic Efficacy of R1antTNF on Lethal Hepatitis Model*—To assess the inhibitory activity and therapeutic effect of R1antTNF *in vivo*, we investigated the protective effect of R1antTNF in the TNF/D-(+)-galactosamine (GalN)-induced hepatitis model. GalN is a hepatotoxin that inhibits transcription and translation in hepatocytes. The combined administration of GalN and TNF causes massive apoptosis of hepatocytes and induces lethal hepatitis (36). In the control group, all mice died within 12 h after a lethal challenge with TNF/GalN (Fig. 5*A*). Co-treatment with R1antTNF improved the survival rate. Especially, in mice co-treated with R1antTNF (270 μg/mouse), the survival rates were 5/6 after 12 h and 3/6 after 24 h (Fig. 5*A*). The surviving mice were still alive several weeks after the treatment. In the control group, the serum levels of ALT, a marker for liver damage, were markedly elevated. In contrast, co-treatment of mice with R1antTNF suppressed the elevation of ALT levels in a dose-dependent manner (Fig. 5*B*). These results demonstrated that R1antTNF had antagonistic activity not only *in vitro* but also *in vivo*, and exhibited remarkable inhibitory effect on hepatitis.

**TABLE 3**
**Binding properties of R1antTNF**

| Receptor | Kinetic parameter | wtTNF | R1antTNF |
|---|---|---|---|
| hTNFR1 | $k_{on}$ ($\times 10^5$ $M^{-1}s^{-1}$)[a] | 3.6 ± 2.9 | 8.3 ± 0.1 |
| | $k_{off}$ ($\times 10^{-4}$ $s^{-1}$)[b] | 5.0 ± 1.3 | 28.7 ± 5.9 |
| | $K_D$ ($\times 10^{-9}$ M)[c] | 1.4 ± 2.7 | 3.5 ± 1.8 |
| hTNFR2 | $k_{on}$ ($\times 10^5$ $M^{-1}s^{-1}$) | 7.0 ± 3.2 | 0.000001 ± 0.0 |
| | $k_{off}$ ($\times 10^{-4}$ $s^{-1}$) | 14.5 ± 4.9 | 0.1 ± 0.0 |
| | $K_D$ ($\times 10^{-9}$ M) | 2.1 ± 1.1 | 92,900 ± 96.1 |
| mTNFR1 | $k_{on}$ ($\times 10^5$ $M^{-1}s^{-1}$) | 2.5 ± 0.0 | 18.7 ± 0.2 |
| | $k_{off}$ ($\times 10^{-4}$ $s^{-1}$) | 1.9 ± 0.3 | 96.6 ± 0.8 |
| | $K_D$ ($\times 10^{-9}$ M) | 0.8 ± 0.4 | 5.2 ± 0.5 |

[a] $k_{on}$ is the association kinetic constant.
[b] $k_{off}$ is the dissociation kinetic constant.
[c] $K_D$ is the equilibrium dissociation constant. Kinetic parameters for each TNF was calculated from the respective sensorgram by BIAevaluation 3.0 software.

*Binding Mode and Affinity of R1antTNF*—The dissociation constant ($K_d$) of R1antTNF binding to hTNFR1 was very similar to that of the wtTNF (Table 2), whereas the R1antTNF (mutTNF-T2) has no bioactivity through TNFR1 (Fig. 2*A*). We predicted that the binding modes of the wtTNF and R1antTNF to the TNFR1 are different, resulting in different biological activities. To quantify the altered binding mode of R1antTNF, we examined the binding kinetics of the R1antTNF for the mTNFR1, hTNFR1, and hTNFR2 using the surface plasmon resonance technique (Table 3). Indeed, the dissociation kinetic constants ($k_{off}$) of the R1antTNF for the human and mouse

TNFR1 (hTNFR1, $16.0 \times 10^{-4}\ s^{-1}$; mTNFR1, $37.0 \times 10^{-4}\ s^{-1}$) were clearly higher than those of the wtTNF (hTNFR1, $3.0 \times 10^{-4}\ s^{-1}$; mTNFR1, $1.5 \times 10^{-4}\ s^{-1}$). The association kinetic constants ($k_{on}$) of the R1antTNF for the human and mouse TNFR1 were also higher than those of the wtTNF. These results suggest that the R1antTNF interacts with the TNFR1 by repeating very quick binding and dissociation, and has a binding mode that is different from that of the wtTNF.

**TABLE 4**
**X-ray data collection and refinement statistics (molecular replacement)**

| Crystal | R1antTNF |
|---|---|
| **Data collection** | |
| Space group | $P2_12_12_1$ |
| Cell dimensions | |
| *a*, *b*, *c* (Å) | 66.56, 66.97, 103.56 |
| Resolution (Å) | 50.0-1.80 (1.86-1.80)[a] |
| $R_{merge}$ | 0.063 (0.484) |
| $I/\sigma I$ | 36.8 (2.71) |
| Completeness (%) | 99.6 (96.1) |
| Redundancy | 7.1 (6.0) |
| **Refinement** | |
| Resolution (Å) | 41.0-1.80 |
| No. of reflections | 42,155 |
| $R_{work}/R_{free}$ | 19.8/23.9 |
| No. of atoms | |
| Protein | 3384 |
| Water | 237 |
| Root mean squares deviations | |
| Bond lengths (Å) | 0.00840 |
| Bond angles (°) | 1.47 |

[a] Highest resolution shell is shown in parentheses.

*Crystal Structure of R1antTNF*—To understand the structural basis for the different binding mode and absence of signal transduction via the R1antTNF, we examined the structure of R1antTNF by x-ray crystallography. After establishing crystallization conditions, good quality crystals of R1antTNF were obtained. The R1antTNF crystal size was $\sim 0.2 \times 0.2 \times 0.4\ mm^3$. X-ray diffraction data were collected in SPring-8 (the large synchrotron radiation facility in Japan). Analysis of these data show that the space group is $P2_12_12_1$, and the lattice constants are $a = 64.56$, $b = 66.97$, and $c = 103.56$ Å (Table 4). The R1antTNF structure was further refined using CNS. Results of the model validation using the Procheck were as follows: 88.4% residues in the most favored regions; 11.0% residues in the additional allowed regions; 0.6% residues in the generously allowed regions; and 0.0% residues in the disallowed regions. The overall structure of the R1antTNF was a trimer (Fig. 6*A*) (PDB code 2E7A), which was similar to that of the wtTNF trimer (Fig. 6*B*) (PDB code 1TNF) (37). Interestingly, structural superposition of the R1antTNF and human wtTNF showed extraordinary similarity (root mean square deviation 1.17 Å for 444 C-$\alpha$ atoms) of their overall structures despite their contradictory functions (Fig. 6*C*). It is believed that the TNF signaling is initiated by the formation of a complex with the three TNFRs on the cell surface. However, the fact that the R1antTNF did not transduce signaling suggests that there might be other structural differences between the wtTNF and R1antTNF.

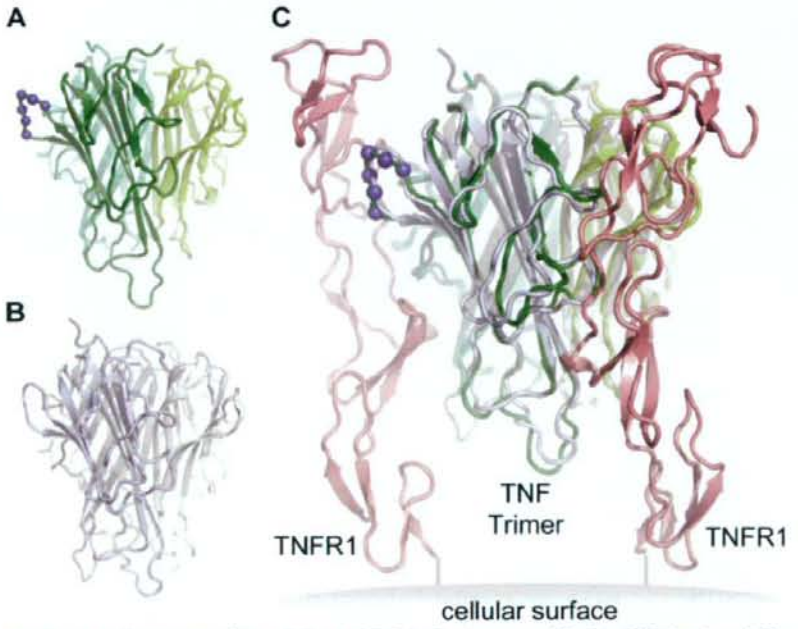


FIGURE 6. **Overall structures of R1antTNF and wtTNF.** *A*, refined structure of the R1antTNF trimer (*green*). *Blue spheres* show the mutated residues(amino acids 84–89) in R1antTNF. This structure is registered in the PDB (PDB code 2E7A). *B*, structure of the wtTNF trimer (*gray*). This structure has been published, and its PDB code is 1TNF. *C*, model structures of the TNF-TNFR1 complexes. Each TNF is superposed on the LT-$\alpha$ derived from the LT-$\alpha$-TNFR1 complex (PDB code 1TNR). TNF binds to three R1 monomers on the cell surface. TNFR1s are shown using *red schematics*. Superposition of the structures of the wtTNF and R1antTNF was performed using the ccp4i program.

## DISCUSSION

TNF, secreted from the site of injury or because of the activation of the immune cells, is involved in the development of inflammatory diseases, and it predominantly activates TNFR1 (40, 41). The TNFR1 knock-out mice have been reported to be resistant to the onset of several inflammatory diseases, such as sepsis, rheumatoid arthritis, and multiple sclerosis (14, 16, 42). In agreement with this, blocking the interaction between the TNF and TNFR1 has emerged as a powerful and clinically effective therapy for the acute inflammation and autoimmune conditions. In this study, we generated TNFR1-selective antagonistic TNF mutants using a phage library displaying structural variants of human TNF.

Among 10 potential candidates, the mutTNF-T2 (R1antTNF) selectively and strongly bound to the TNFR1 but showed almost no bioactivity. Additionally, we found that R1antTNF most effectively inhibited the wtTNF-induced cell death

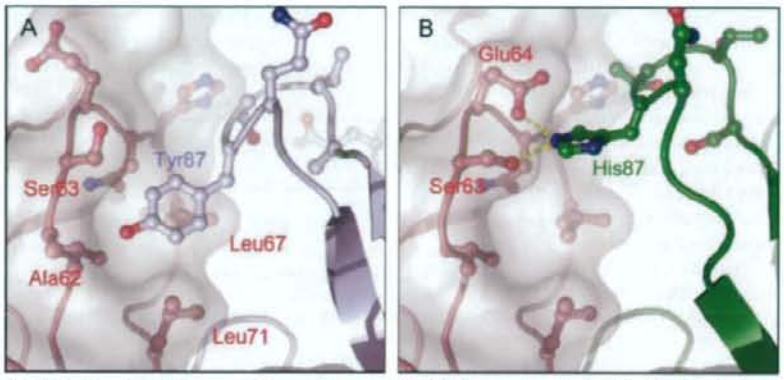


FIGURE 7. **Structural difference between the receptor binding region of the R1antTNF and wtTNF.** *A*, interaction between the wtTNF (*gray*) and TNFR1 (*red*). *White layer* depicts the molecular surface of the TNFR1. Hydrophobic interaction is formed between the Tyr-87 and molecular pocket in the TNFR1 (Leu-67, Leu-71, Ala-62, and Ser-63). *B*, interaction between the R1antTNF (*green*) and TNFR1 (*red*). *Yellow broken lines* show the possible interactions of the R1antTNF His-87 with the receptor Ser-63 and Glu-64. In this simulation, the side chains of each structure were rotated to fit the predicted interaction. Stable structures of these rotamers were constructed using the O program.

(Fig. 3*B*). R1antTNF also clearly inhibited the TNF functions other than cytotoxicity. Interestingly, the ratio between the R1antTNF and wtTNF was 1000-fold or more to obtain 50% inhibition against the wtTNF-induced cytotoxicity and caspase-3/7 activity, whereas the ratio was only about 100-fold or less to obtain 50% inhibition against the wtTNF-induced expression of E-selectin, production of GM-CSF, and NF-κB activation. Intracellular signaling induced by the TNF/TNFR1 interaction is divided into the following two main pathways: (i) the NF-κB pathway, which regulates the expression of adhesion molecules and inflammatory cytokines, and (ii) the caspase cascade, which induces cell death through apoptosis or necrosis (34). Our results suggest that R1antTNF is more antagonistic against the wtTNF function mediated via the NF-κB pathway than via the caspase cascade. In pathological tissues, endogenous TNF induced expression of the cell adhesion molecules and inflammatory cytokines resulting in leukocyte infiltration, which are regulated by NF-κB and are closely related to the development or exacerbation of diseases (43) such as fulminant hepatitis and rheumatoid arthritis. Because the R1antTNF efficiently inhibited the TNF-induced NF-κB activation, it would be of therapeutic value for the treatment of such inflammatory diseases. These cell line or signaling pathway-dependent differences in the inhibitory efficiencies of R1antTNF could be valuable in studying the structural or biological changes caused by the TNF/TNFR1 interactions, which need to be explored further.

We examined the therapeutic effects of R1antTNF in the acute lethal hepatitis model. R1antTNF exhibited the suppressive effect on acute hepatitis. Although the R1antTNF suppressed the elevation of the ALT level in a dose-dependent manner, the survival rate was not significantly improved between the dose 10 μg/mouse *versus* 270 μg/mouse. This discrepancy is likely because the difference in the degree of suppression of the elevated ALT level does not always correlate well with the improvement in the survival rate. Nevertheless, treatment with only 30–270 μg/mouse R1antTNF (30–270-fold excess over wtTNF) significantly suppressed the elevation of ALT levels and reduced the lethal toxicity. Thus, the antagonistic activity of R1antTNF *in vivo* was stronger than expected from the *in vitro* results. The TNF/GalN-mediated activation of TNFR1 not only induces apoptosis and necrosis of hepatocytes but also induces inflammatory responses and secondary responses associated with the cell death (44). Therefore, we believe that the R1antTNF exerted its therapeutic effect by comprehensively inhibiting the TNF/GalN-mediated biological responses, thus blocking the liver failure in the experimental animals. The R1antTNF is also expected to have therapeutic effect in chronic inflammatory disease models, such as in collagen-induced arthritis model and experimental autoimmune encephalomyelitis model. However, the plasma half-life of R1antTNF, like the wtTNF, is very short (12 min). We recently developed a novel PEGylation system that dramatically improved the *in vivo* stability and therapeutic effects of the bioactive proteins (29, 45). We are currently in the process of developing the PEGylated R1antTNF to further enhance its potential anti-inflammatory activity.

To explore the underlying mechanism of the antagonistic activity of R1antTNF, we examined the crystal structure of R1antTNF by x-ray crystallography. Despite close resemblance between the crystal structure of the R1antTNF and wtTNF, the receptor-bound R1antTNF did not transmit any signal via the TNFR1. To further speculate why the R1antTNF showed antagonistic activity, we utilized the superpose program to perform docking simulations with the TNFs and TNFR1 using the crystal structure of the LT-α-TNFR1 complex (PDB code 1TNR) (31). The TNF-TNFR1 model complex suggested that the Tyr-87 of the wtTNF, an essential residue, is buried in a molecular hydrophobic "pocket" of the TNFR1, which houses the receptor residues Leu-67 and Leu-71 that are implicated to maintain the TNF and TNFR1 complex (Fig. 7*A*). Tyr-87 is a highly conserved residue throughout the TNF superfamily, such as LT-α, LT-β and LIGHT, and this discussion is also reflected in the crystal structure of the LT-α-TNFR1 complex (38). Accordingly, site-directed mutagenesis of the Tyr-87 residue of TNF resulted in a dramatic loss of its biological activity and affinities for both TNFRs (39), suggesting that this residue is be essential for TNF function. However, in R1antTNF, the Tyr-87 is replaced with a histidine residue. The structural simulation studies suggested that the His-87 in R1antTNF could interact with the relatively negatively charged Ser-63 and Glu-64 residues on the TNFR1 surface, which probably explains the different binding mode of the R1antTNF as compared with the wtTNF (Fig. 7*B*).

Indeed, the association and dissociation kinetic constants ($k_{on}$ and $k_{off}$, respectively) for the binding of R1antTNF to TNFR1 were considerably higher than those of the wtTNF, indicating a difference in the TNFR1-binding pattern between the wtTNF and R1antTNF (Table 3). The association and dissociation kinetic constants are very important factors in discussing the ligand-receptor interaction and function. It was previously shown that the membrane-bound TNF, but not the soluble TNF, could activate the TNFR2, and the reason for this difference was attributed to the dissociation kinetic constant of the soluble TNF, which was much higher than the membrane-bound TNF (46). Therefore, the inability of R1antTNF to transmit signal and its antagonistic activity are probably because of the higher $k_{on}$ and $k_{off}$ values of R1antTNF for the TNFR1, suggesting that they influenced the stability of the TNF-TNFR1 complex and reduced the continuous binding time required for the signal transmission. In addition, we demonstrated that R1antTNF inhibited the activations of both caspase-3/7 and NF-κB (Fig. 5, *A* and *B*), which are mediated via two distinct intracellular signaling complexes. TNF/TNFR1-mediated signaling requires sequential formation of the following two receptor complexes: the complex I is involved in the recruitment of TRADD, RIP1, and TRAF2 leading to the NF-κB activation, whereas the consequent complex II is involved in internalization, post-translational modifications, and recruitment of FADD and caspase-8 initiating apoptosis (47). Together, these results suggest that R1antTNF blocked the TNF-mediated signal transmission by binding to TNFR1 in a rapid association/dissociation cycle, thereby inhibiting the formation of the intracellular complexes. However, more detailed investigations, such as detection of these intracellular complexes and their internalization, other TNF/TNFR1-mediated signaling, and analysis of the complex structure of the R1antTNF and TNFR1, are required to elucidate exactly how the R1antTNF exhibits its TNFR1 antagonistic activity.

We succeeded in developing the first mutant form of the human TNF with TNFR1-selective antagonistic activity by using a unique combinatorial phage-based technique. Existing TNF blockers, *i.e.* etanercept and infliximab, are widely used in the treatment of rheumatoid arthritis and Crohn disease (5). But these drugs, which prevent TNF binding on both TNF receptor types, can cause serious side effects, such as mycobacterial infections and hepatitis B virus infection (48). Although TNFR1 is believed to be important for immunological responses (42), TNFR2 is thought to be also important for antiviral resistance and is effective for controlling the mycobacterial infection by affecting the membrane-bound TNF stimulation (18, 49). Therefore, this mutant TNF, R1antTNF, might be a new therapeutic drug with reduced side effects. We are currently evaluating not only the therapeutic effect of R1antTNF on rheumatoid arthritis or experimental encephalomyelitis model, and but also its side effects such as mycobacterial and virus infection. Finally, our studies demonstrate the feasibility of generating TNF receptor subtype-selective antagonistic mutants by comprehensive substitution of sets of amino acids in the wild-type ligand proteins. Our data also suggest that this combinatorial biosynthetic strategy using the bioactive protein as the "lead protein" is very effective in creating receptor-specific agonists and antagonists, and we believe that this approach will generate protein drugs of improved therapeutic value.

*Acknowledgment—We thank E. C. Gabazza for discussions and critical reading of the manuscript.*

## REFERENCES


1. Aggarwal, B. B. (2003) *Nat. Rev. Immunol.* **3,** 745–756
2. Aderka, D., Engelmann, H., Maor, Y., Brakebusch, C., and Wallach, D. (1992) *J. Exp. Med.* **175,** 323–329
3. Feldmann, M., and Maini, R. N. (2003) *Nat. Med.* **9,** 1245–1250
4. Muto, Y., Nouri-Aria, K. T., Meager, A., Alexander, G. J., Eddleston, A. L., and Williams, R. (1988) *Lancet* **2,** 72–74
5. Feldmann, M. (2002) *Nat. Rev. Immunol.* **2,** 364–371
6. Goldbach-Mansky, R., and Lipsky, P. E. (2003) *Annu. Rev. Med.* **54,** 197–216
7. Brown, S. L., Greene, M. H., Gershon, S. K., Edwards, E. T., and Braun, M. M. (2002) *Arthritis Rheum.* **46,** 3151–3158
8. Keane, J., Gershon, S., Wise, R. P., Mirabile-Levens, E., Kasznica, J., Schwieterman, W. D., Siegel, J. N., and Braun, M. M. (2001) *N. Engl. J. Med.* **345,** 1098–1104
9. Nathan, D. M., Angus, P. W., and Gibson, P. R. (2006) *J. Gastroenterol. Hepatol.* **21,** 1366–1371
10. Shakoor, N., Michalska, M., Harris, C. A., and Block, J. A. (2002) *Lancet* **359,** 579–580
11. Sicotte, N. L., and Voskuhl, R. R. (2001) *Neurology* **57,** 1885–1888
12. Aggarwal, B. B., Eessalu, T. E., and Hass, P. E. (1985) *Nature* **318,** 665–667
13. Leist, M., Gantner, F., Jilg, S., and Wendel, A. (1995) *J. Immunol.* **154,** 1307–1316
14. Mori, L., Iselin, S., De Libero, G., and Lesslauer, W. (1996) *J. Immunol.* **157,** 3178–3182
15. Liu, J., Marino, M. W., Wong, G., Grail, D., Dunn, A., Bettadapura, J., Slavin, A. J., Old, L., and Bernard, C. C. (1998) *Nat. Med.* **4,** 78–83
16. Kassiotis, G., and Kollias, G. (2001) *J. Exp. Med.* **193,** 427–434
17. Fremond, C., Allie, N., Dambuza, I., Grivennikov, S. I., Yeremeev, V., Quesniaux, V. F., Jacobs, M., and Ryffel, B. (2005) *Respir. Res.* **6,** 136
18. Olleros, M. L., Guler, R., Corazza, N., Vesin, D., Eugster, H. P., Marchal, G., Chavarot, P., Mueller, C., and Garcia, I. (2002) *J. Immunol.* **168,** 3394–3401
19. Grell, M., Becke, F. M., Wajant, H., Mannel, D. N., and Scheurich, P. (1998) *Eur. J. Immunol.* **28,** 257–263
20. Kafrouni, M. I., Brown, G. R., and Thiele, D. L. (2003) *J. Leukocyte Biol.* **74,** 564–571
21. Kim, E. Y., Priatel, J. J., Teh, S. J., and Teh, H. S. (2006) *J. Immunol.* **176,** 1026–1035
22. Engelmann, H., Holtmann, H., Brakebusch, C., Avni, Y. S., Sarov, I., Nophar, Y., Hadas, E., Leitner, O., and Wallach, D. (1990) *J. Biol. Chem.* **265,** 14497–14504
23. Carter, P. H., Scherle, P. A., Muckelbauer, J. K., Voss, M. E., Liu, R. Q., Thompson, L. A., Tebben, A. J., Solomon, K. A., Lo, Y. C., Li, Z., Strzemienski, P., Yang, G., Falahatpisheh, N., Xu, M., Wu, Z., Farrow, N. A., Ramnarayan, K., Wang, J., Rideout, D., Yalamoori, V., Domaille, P., Underwood, D. J., Trzaskos, J. M., Friedman, S. M., Newton, R. C., and Decicco, C. P. (2001) *Proc. Natl. Acad. Sci. U. S. A.* **98,** 11879–11884
24. Murali, R., Cheng, X., Berezov, A., Du, X., Schon, A., Freire, E., Xu, X., Chen, Y. H., and Greene, M. I. (2005) *Proc. Natl. Acad. Sci. U. S. A.* **102,** 10970–10975
25. Vandenabeele, P., Declercq, W., Vercammen, D., Van de Craen, M., Grooten, J., Loetscher, H., Brockhaus, M., Lesslauer, W., and Fiers, W. (1992) *J. Exp. Med.* **176,** 1015–1024
26. Tsutsumi, Y., Kihira, T., Tsunoda, S., Kanamori, T., Nakagawa, S., and Mayumi, T. (1995) *Br. J. Cancer* **71,** 963–968
27. Barbara, J. A., Smith, W. B., Gamble, J. R., Van Ostade, X., Vandenabeele,

P., Tavernier, J., Fiers, W., Vadas, M. A., and Lopez, A. F. (1994) *EMBO J.* **13,** 843–850
28. Brunetti, C. R., Paulose-Murphy, M., Singh, R., Qin, J., Barrett, J. W., Tardivel, A., Schneider, P., Essani, K., and McFadden, G. (2003) *Proc. Natl. Acad. Sci. U. S. A.* **100,** 4831–4836
29. Yamamoto, Y., Tsutsumi, Y., Yoshioka, Y., Nishibata, T., Kobayashi, K., Okamoto, T., Mukai, Y., Shimizu, T., Nakagawa, S., Nagata, S., and Mayumi, T. (2003) *Nat. Biotechnol.* **21,** 546–552
30. Potterton, E., Briggs, P., Turkenburg, M., and Dodson, E. (2003) *Acta Crystallogr. Sect. D. Biol. Crystallogr.* **59,** 1131–1137
31. Banner, D. W., D'Arcy, A., Janes, W., Gentz, R., Schoenfeld, H. J., Broger, C., Loetscher, H., and Lesslauer, W. (1993) *Cell* **73,** 431–445
32. Jones, T. A., Zou, J. Y., Cowan, S. W., and Kjeldgaard, M. (1991) *Acta Crystallogr. Sect. A.* **47,** 110–119
33. Brunger, A. T., Adams, P. D., Clore, G. M., DeLano, W. L., Gros, P., Grosse-Kunstleve, R. W., Jiang, J. S., Kuszewski, J., Nilges, M., Pannu, N. S., Read, R. J., Rice, L. M., Simonson, T., and Warren, G. L. (1998) *Acta Crystallogr. Sect. D. Biol. Crystallogr.* **54,** 905–921
34. Chen, G., and Goeddel, D. V. (2002) *Science* **296,** 1634–1635
35. Mackay, F., Loetscher, H., Stueber, D., Gehr, G., and Lesslauer, W. (1993) *J. Exp. Med.* **177,** 1277–1286
36. Hishinuma, I., Nagakawa, J., Hirota, K., Miyamoto, K., Tsukidate, K., Yamanaka, T., Katayama, K., and Yamatsu, I. (1990) *Hepatology* **12,** 1187–1191
37. Eck, M. J., and Sprang, S. R. (1989) *J. Biol. Chem.* **264,** 17595–17605
38. Harrop, J. A., McDonnell, P. C., Brigham-Burke, M., Lyn, S. D., Minton, J., Tan, K. B., Dede, K., Spampanato, J., Silverman, C., Hensley, P., DiPrinzio, R., Emery, J. G., Deen, K., Eichman, C., Chabot-Fletcher, M., Truneh, A., and Young, P. R. (1998) *J. Biol. Chem.* **273,** 27548–27556
39. Zhang, X. M., Weber, L., and Chen, M. J. (1992) *J. Biol. Chem.* **267,** 24069–24075
40. Ruuls, S. R., Hoek, R. M., Ngo, V. N., McNeil, T., Lucian, L. A., Janatpour, M. J., Korner, H., Scheerens, H., Hessel, E. M., Cyster, J. G., McEvoy, L. M., and Sedgwick, J. D. (2001) *Immunity* **15,** 533–543
41. Grell, M., Douni, E., Wajant, H., Lohden, M., Clauss, M., Maxeiner, B., Georgopoulos, S., Lesslauer, W., Kollias, G., Pfizenmaier, K., and Scheurich, P. (1995) *Cell* **83,** 793–802
42. Rothe, J., Lesslauer, W., Lotscher, H., Lang, Y., Koebel, P., Kontgen, F., Althage, A., Zinkernagel, R., Steinmetz, M., and Bluethmann, H. (1993) *Nature* **364,** 798–802
43. Zhou, A., Scoggin, S., Gaynor, R. B., and Williams, N. S. (2003) *Oncogene* **22,** 2054–2064
44. Nagaki, M., Sugiyama, A., Osawa, Y., Naiki, T., Nakashima, S., Nozawa, Y., and Moriwaki, H. (1999) *J. Hepatol.* **31,** 997–1005
45. Kamada, H., Tsutsumi, Y., Sato-Kamada, K., Yamamoto, Y., Yoshioka, Y., Okamoto, T., Nakagawa, S., Nagata, S., and Mayumi, T. (2003) *Nat. Biotechnol.* **21,** 399–404
46. Krippner-Heidenreich, A., Tubing, F., Bryde, S., Willi, S., Zimmermann, G., and Scheurich, P. (2002) *J. Biol. Chem.* **277,** 44155–44163
47. Micheau, O., and Tschopp, J. (2003) *Cell* **114,** 181–190
48. Gomez-Reino, J. J., Carmona, L., Valverde, V. R., Mola, E. M., and Montero, M. D. (2003) *Arthritis Rheum.* **48,** 2122–2127
49. Saunders, B. M., Tran, S., Ruuls, S., Sedgwick, J. D., Briscoe, H., and Britton, W. J. (2005) *J. Immunol.* **174,** 4852–4859

British Journal of Pharmacology (2008) 153, 1143–1152

0007–1188/08 $30.00
www.brjpharmacol.org

# RESEARCH PAPER

# Comparative study on transduction and toxicity of protein transduction domains

T Sugita[1,2], T Yoshikawa[1], Y Mukai[1,2], N Yamanada[1,2], S Imai[1,2], K Nagano[1,2], Y Yoshida[1,3], H Shibata[1], Y Yoshioka[1,4], S Nakagawa[2], H Kamada[1,4], S-i Tsunoda[1,4] and Y Tsutsumi[1,3,4]

[1]*Laboratory of Pharmaceutical Proteomics, National Institute of Biomedical Innovation (NIBIO), Ibaraki, Osaka, Japan;* [2]*Department of Biotechnology and Therapeutics, Graduate School of Pharmaceutical Sciences, Osaka University, Suita, Osaka, Japan;* [3]*Department of Biomedical Innovation, Graduate School of Pharmaceutical Sciences, Osaka University, Suita, Osaka, Japan and* [4]*The Center for Advanced Medical Engineering and Informatics, Osaka University, Suita, Osaka, Japan*

**Background and purpose:** Protein transduction domains (PTDs), such as Tat, antennapedia homeoprotein (Antp), Rev and VP22, have been extensively utilized for intracellular delivery of biologically active macromolecules *in vitro* and *in vivo*. There is little known, however, about the relative transduction efficacy, cytotoxicity and internalization mechanism of individual PTDs.
**Experimental approach:** We examined the cargo delivery efficacies of four major PTDs (Tat, Antp, Rev and VP22) and evaluated their toxicities and cell internalizing pathways in various cell lines.
**Key results:** The relative order of the transduction efficacy of these PTDs conjugated to fluorescein was Rev > Antp > Tat > VP22, independent of cell type (HeLa, HaCaT, A431, Jurkat, MOLT-4 and HL60 cells). Antp produced significant toxicity in HeLa and Jurkat cells, and Rev produced significant toxicity in Jurkat cells. Flow cytometric analysis demonstrated that the uptake of PTD–fluorescein conjugate was dose-dependently inhibited by methyl-β-cyclodextrin, cytochalasin D and amiloride, indicating that all four PTDs were internalized by the macropinocytotic pathway. Accordingly, in cells co-treated with 'Tat-fused' endosome-disruptive HA2 peptides (HA2-Tat) and independent PTD-fluorescent protein conjugates, fluorescence spread throughout the cytosol, indicating that all four PTDs were internalized into the same vesicles as Tat.
**Conclusions and implications:** These findings suggest that macropinocytosis-dependent internalization is a crucial step in PTD-mediated molecular transduction. From the viewpoint of developing effective and safe protein transduction technology, although Tat was the most versatile carrier among the peptides studied, PTDs should be selected based on their individual characteristics.
*British Journal of Pharmacology* (2008) **153**, 1143–1152; doi:10.1038/sj.bjp.0707678; published online 28 January 2008

**Keywords:** protein transduction domains; Tat; antennapedia; Rev; VP22; macropinocytosis

**Abbreviations:** PTD, protein transduction domain; Antp, antennapedia

## Introduction

A strong focus of research in the post-genomic era is the development of effective therapies for refractory diseases such as cancer and neurodegenerative syndromes (Rhodes and Chinnaiyan, 2005; Brusic *et al.*, 2007; Drabik *et al.*, 2007). Because the therapeutic targets of these diseases generally exist inside the cell, it is necessary to establish drug delivery methods that transfer macromolecules, such as therapeutic proteins or peptide-based drugs, across the cellular membrane (Nori and Kopecek, 2005; Murriel and Dowdy, 2006; Borsello and Forloni, 2007).

Correspondence: Dr S-i Tsunoda, Laboratory of Pharmaceutical Proteomics, National Institute of Biomedical Innovation (NIBIO), 7-6-8 Saito-Asagi, Ibaraki, Osaka 597-0085, Japan.
E-mail: tsunoda@nibio.go.jp
Received 9 November 2007; accepted 4 December 2007; published online 28 January 2008

Protein transduction is a recently developed method for delivering biologically active proteins directly into mammalian cells with high efficiency (Hawiger, 1999; Schwarze *et al.*, 2000). Recombinant technology is used to modify the biophysical properties of proteins and peptides, particularly with respect to their cell permeability, using the so-called protein transduction domains (PTDs) (Nagahara *et al.*, 1998; Rojas *et al.*, 1998; Schwarze *et al.*, 1999). The HIV-1-derived Tat peptide renders various macromolecules cell permeable. Although the initial reports suggested that protein transduction is energy and temperature independent, these characteristics are now mostly attributed to phenomena such as fixation artefacts (Richard *et al.*, 2003). More recent data indicate that basic PTDs such as Tat enter the cells through a macropinocytotic pathway that is universally active in all cells (Wadia *et al.*, 2004; Kaplan *et al.*, 2005). A series of events involves Tat attachment to an anionic cell surface,

followed by the association of these complexes with lipid rafts, which triggers dynamin-independent macropinocytosis. After internalization, the endosome pH falls and Tat apparently destabilizes the membranes, which results in a small amount of the endosome contents escaping into the cytosol. The released fraction of Tat can then exert its biologic activity. Consistent with this model, Tat delivery is enhanced by the influenza virus haemagglutinin fusogenic motif, which further destabilizes endosomal membranes at a low pH (Han *et al.*, 2001; Skehel *et al.*, 2001). In cells cotreated with Tat-conjugated HA2 (HA2-Tat), a greater proportion of endocytosed Tat-fused Cre recombinase escapes into the cytoplasm (Wadia *et al.*, 2004). Other studies suggest that certain cell types might incorporate Tat constructs by clathrin- or caveolin-dependent endocytosis, raising the possibility that transport varies according to the cargo or cell type (Ferrari *et al.*, 2003; Fittipaldi *et al.*, 2003; Richard *et al.*, 2005). In addition to the basic Tat peptide, there are other proteins (fragments), such as antennapedia (Antp), Rev and VP22, that enhance cellular uptake of proteins (Table 1) (Derossi *et al.*, 1994; Elliott and O'Hare, 1997; Futaki *et al.*, 2001; Joliot and Prochiantz, 2004). These four well-known PTDs facilitate the delivery of various biomacromolecules into the cell, but few studies have examined their relative efficacy.

In the present study, we evaluated the potency and internalizing pathway of four major PTDs to optimize protein transduction technology and to clarify the mechanisms of action. We also evaluated the cytotoxicity of these four PTDs as this is crucial to their utility as effective biomacromolecule carriers. These analyses may help not only to elucidate the mechanism by which the four peptides facilitate the cellular uptake of biomacromolecules, but also provide criteria for their proper use.

## Materials and methods

*Cell lines*

HeLa cells (human cervical carcinoma cells) and A431 cells (human epithelial carcinoma cells) were obtained from the American Type Culture Collection (Manassas, VA, USA). HaCaT cells (human keratinocyte cells) were kindly provided by Dr S Inui, Osaka University. Jurkat cells (human leukaemia cells) and MOLT-4 cells (human leukaemia cells) were kindly provided by Hayashibara Biochemical Laboratories Inc. (Okayama, Japan). HL60 cells (human promyelocytic leukaemia cells) were obtained from the Japanese Collection of Research Bioresources (JCRB; Osaka, Japan). HeLa cells were cultured in minimal essential medium (MEMα; Wako Pure Chemicals, Osaka, Japan) medium supplemented with 10% fetal bovine serum (FBS) and antibiotics. A431 cells and HaCaT cells were maintained in Dulbecco's modified Eagle's medium (Wako Pure Chemicals) supplemented with 10% FBS, 1% L-glutamine and antibiotics. Jurkat cells and MOLT-4 cells were maintained in RPMI-1640 medium (Wako Pure Chemicals) supplemented with 10% FBS and antibiotics. HL60 cells were maintained in RPMI-1640 medium (Wako Pure Chemicals) supplemented with 20% FBS and antibiotics. All cells were cultured at 37 °C in 5% $CO_2$.

**Table 1** Protein sequences of the PTDs evaluated

| *PTD* | *Origin* | *Sequence* | *pI* |
|---|---|---|---|
| Tat | HIV-1 | GRKKRRQRRRPPQ | 12.70 |
| Antp | *Drosophila* | RQIKIWFQNRRMKWKK | 12.31 |
| Rev | HIV-1 | TRQARRNRRRRWRERQR | 12.60 |
| VP22 | HSV | NAKTRRHERRRKLAIER | 12.01 |

The basic amino acids in each sequence are shown in bold.

*Synthetic peptides*

All peptides used in this study were purchased from the Toray Research Center Inc. (Tokyo, Japan) and had purities above 90%, which was confirmed by high-performance liquid chromatography analysis and mass spectroscopy. The sequences of these peptides were GRKKRRQRRRPPQK-FAM (FAM = carboxyfluorescein) for Tat-conjugated FAM (Tat-FAM), RQIKIWFQNRRMKWKKK-FAM for Antp-conjugated FAM (Antp-FAM), TRQARRNRRRRWRERQRK-FAM for Rev-conjugated FAM (Rev-FAM), NAKTRRHERRRKLAIERK-FAM for VP22-conjugated FAM (VP22-FAM), YGRKKRRQRRRK-biotin for Tat-conjugated biotin, RQIKIWFQNRRMKWKKK-biotin Antp-conjugated biotin, TQRARRNRRRRWRERQRK-biotin for Rev-conjugated biotin, NAKTRRHERRRKLAIERK-biotin for VP22-conjugated biotin and GLFEAIEGFIENGWEGMIDGWY GYGRKKRRQRRR for HA2-conjugated Tat (HA2-Tat). The individual PTD sequences are underlined.

*Flow cytometric analysis*

HeLa cells, HaCaT cells and A431 cells were cultured in 24-well plates (Nalge Nunc International, Naperville, IL, USA) at $5.0 \times 10^4$ cells per well in culture medium and incubated for 24 h at 37 °C. Jurkat cells, MOLT-4 cells and HL60 cells were cultured in 24-well plates (Nalge Nunc International) at $1.0 \times 10^5$ cells per well in Opti-MEM I (Invitrogen, Carlsbad, CA, USA). After aspirating the media, FAM-conjugated PTD (PTD-FAM) (10 μM) was added to the cells in Opti-MEM I and the culture dishes were incubated for an additional 3 h. Following incubation, the cells were washed with phosphate-buffered saline and incubated for 5 min with 0.1% trypsin to detach them and to remove surface-bound peptides. After incubation, 2 vol of 10% FBS-containing culture medium was added to stop the trypsin activity and to detach the cells completely. The cell suspension was centrifuged at 800 *g*, washed with phosphate-buffered saline, centrifuged again and resuspended in 500 μl of 0.4% paraformaldehyde. Fluorescence was analysed on a FACSCalibur flow cytometer, and data were analysed using CellQuest software (both from Becton Dickinson, San Jose, CA, USA). In the low-temperature uptake experiment, cells were preincubated at 4 °C for 1 h in Opti-MEM I prior to adding the PTDs, and all buffers and solutions were equilibrated to 4 °C. To analyse the internalization mechanism, HeLa cells were pretreated for 30 min in Opti-MEM I medium with 0–5 mM methyl-β-cyclodextrin, 0–2.5 μM

cytochalasin D or 0–5 mM amiloride (all from Sigma-Aldrich, St Louis, MO, USA). After the PTD-FAMs were added, cells were maintained for 1 h (30 min for amiloride) in the presence of inhibitors and washed several times with phosphate-buffered saline. As a control, the cellular uptake of transferrin fluorescein isothiocyanate (Invitrogen) was also monitored.

*Cell proliferation assay*

Cell viability was determined using a WST-8 assay kit (Nacalai Tesque, Kyoto, Japan) according to the manufacturer's instructions. The assay is based on the cleavage of the tetrazolium salt WST-8 to formazan by cellular mitochondrial dehydrogenase. HeLa cells were cultured in 96-well plates (Nalge Nunc International) at $5.0 \times 10^3$ cells per well in MEMα and incubated for 24 h at 37 °C. Jurkat cells were cultured in 96-well plates at $1.0 \times 10^4$ cells per well in Dulbecco's modified Eagle's medium. The cells were treated with various concentrations of PTD-biotin. After 24 h incubation, cell viability was measured using the WST-8 assay kit.

*Membrane integrity assay*

The lactate dehydrogenase (LDH) leakage assay was used to quantify the membrane integrity of the PTD-treated cells. This assay detects the amount of LDH released into the culture media as a result of plasma membrane disruption after PTD treatment. HeLa cells were cultured in 96-well plates (Nalge Nunc International) at $5.0 \times 10^3$ cells per well in MEMα and incubated for 24 h at 37 °C. Jurkat cells were cultured in 96-well plates at $1.0 \times 10^4$ cells per well in Dulbecco's modified Eagle's medium. Each cell type was treated with various concentrations of PTD-biotin. After 3 h incubation, the LDH release activity of the peptides was measured using an LDH cytotoxicity test (Wako) according to the manufacturer's instructions.

*Expression and purification of PTD-fused Venus protein*

The Venus (variant of yellow fluorescent protein) DNA sequence was kindly provided by Dr A Miyawaki (RIKEN Brain Science Institute). The Tat-Venus DNA sequence was amplified by PCR. At the 5′ end, the primer sequence 5′-TTTAAGAAGGAGATATACATATGGCTTACGGTCGTAAAAAA CGTCGCCAGCGTCGCCGTGGTGGCGGCGGTTCCCTCGA GCACCACCATCACCACCATGTGAGCAAGGGCGAGGAGC TGTTCAC-3′ introduced an *Nde* I site and Tat sequence and at the 3′ end, the primer sequence 5′-GCTTTGTTAGCAG CCGAATTCTTACTTGTACAGCTCGTCCATGCCGAGAGTGA TC-3′ introduced an *Eco* RI site. The PCR product was digested with *Nde* I and *Eco* RI and inserted into a protein expression plasmid. Other plasmids expressing Antp-, Rev- or VP22-Venus recombinant proteins were constructed by replacing the Tat-coding region in the Tat-Venus plasmid with the Antp, Rev or VP22 sequences using the *Nde* I and *Xho* I restriction sites. These sequences were obtained by annealing the following oligonucleotides with protruding single-strand DNA corresponding to the *Nde* I and *Xho* I sites: Antp sense, 5′-TATGGCTCGTCAGATCAAAATCTGGTTCCA GAATCGTCGTATGAAGTGGAAAAAGGTGGCGGCGGTTC CC-3′; Antp antisense, 5′-TCGAGGGAACCGCCGCCACCTT TTTTCCACTTCATACGACGATTCTGGAACCAGATTTTGATC TGACGAGCCA-3′; Rev sense, 5′-TATGGCTACCCGTCAGGC TCGTCGTAATCGTCGTCGTCGTTGGCGTGAACGTCAGCGT GGTGGCGGCGGTTCCC-3′; Rev antisense, 5′-TCGAGGGAA CCGCCGCCACCACGCTGACGTTCACGCCAACGACGACGA CGATTACGACGAGCCTGACGGGTAGCCA-3′; VP22 sense, 5′-TATGGCTAACGCTAAAACCCGTCGTCACGAACGTCGTCG TAAACTGGCTATCGAACGTGGTGGCGGCGGTTCCC-3′; VP22 antisense, 5′-TCGAGGGAACCGCCGCCACCACGTTCGATAG CCAGTTTACGACGACGTTCGTGACGACGGGTTTTAGCGT TAGCCA-3′. The plasmids, except for the Antp-Venus expression vector, were transformed into *Escherichia coli* BL21 Star (DE3) (Invitrogen). The Antp-Venus-expressing vector was transformed into BL21 Star (DE3), in which the plasmid-expressing chaperone (pGro7) was pretransformed. Transformed *E. coli* was cultured and the cell paste was suspended in BugBuster Master Mix (Novagen, Darmstadt, Germany) and centrifuged. PTD-Venus was recovered in the supernatant and purified by His-tag affinity purification and gel filtration chromatography.

*Confocal laser scanning microscopy analysis*

HeLa cells were cultured on Lab-Tek II Chambered Coverglass (Nalge Nunc International) at $3.0 \times 10^4$ cells per well in MEMα supplemented with 10% FBS and incubated for 24 h at 37 °C. Internalization of PTD-FAM or PTD-Venus was performed as follows: HeLa cells were treated with PTD-FAM or PTD-Venus (10 μM) in Opti-MEM I containing 100 ng ml$^{-1}$ Hoechst 33342 (Invitrogen) and 6 μg ml$^{-1}$ FM4-64 (Invitrogen). After incubation at 37 °C for 3 h, the medium was exchanged with fresh medium and fluorescence was observed by confocal laser scanning microscopy (Leica Microsystems GmbH, Wetzlar, Germany) without cell fixation. For cotreatment with HA2-Tat, HeLa cells were cotreated with PTD-FAM (10 μM) and HA2-Tat (2 μM) in Opti MEM I containing 100 ng ml$^{-1}$ Hoechst 33342. After incubation at 37 °C for 3 h, the medium was exchanged with fresh medium and fluorescence was observed by confocal laser scanning microscopy without cell fixation.

## Results

*Comparison of transduction efficiency and cytotoxicity of four PTDs*

To confirm the intracellular translocation activity of the four selected PTDs, we evaluated the transduction efficiency of Tat-, Antp-, Rev- and VP22-FAM in six cell lines (adherent: HeLa, HaCaT and A431 cells; nonadherent: Jurkat, MOLT-4 and HL60 cells) using flow cytometric analysis (Figure 1). These PTDs contain a large number of basic amino acids (Table 1) and their cationic properties are thought to be important for cell membrane penetration (Futaki *et al.*, 2001; Chauhan *et al.*, 2007). Their positive charge, however, causes them to adsorb nonspecifically to negatively charged cell

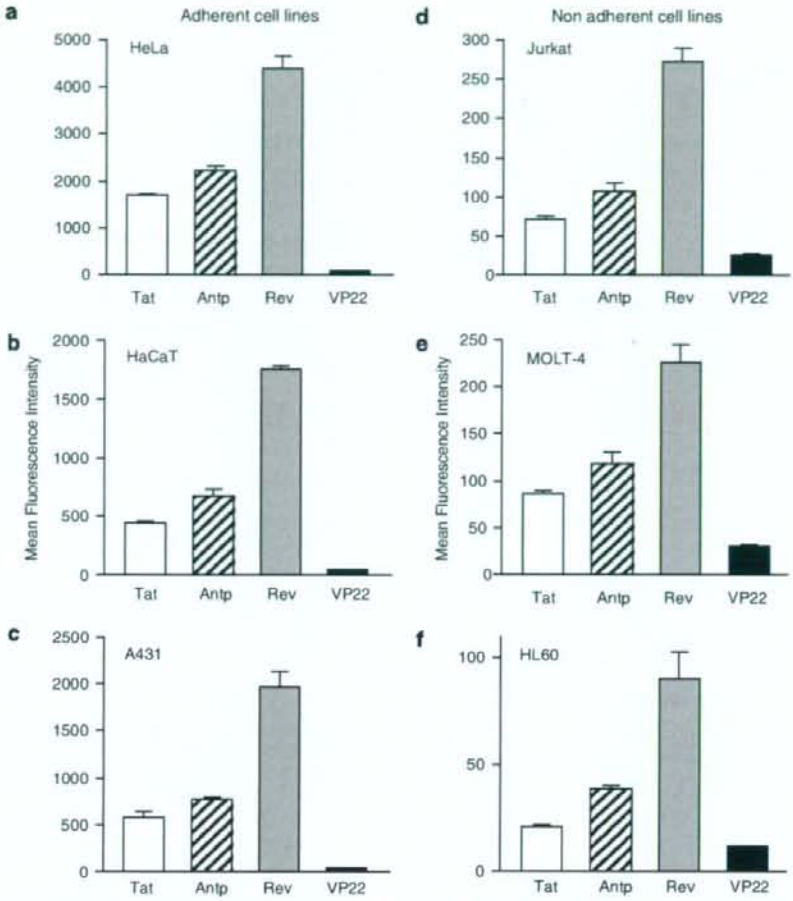


**Figure 1** Comparison of the cellular uptake of protein transduction domains (PTDs). FAM-labelled Tat (white column), antennapedia (Antp; hatched column), Rev (grey column) and VP22 (black column) were incubated with six cell lines: HeLa (**a**), HaCaT (**b**), A431 (**c**), Jurkat (**d**), MOLT-4 (**e**) and HL60 (**f**) at 10 μM for 3 h. After trypsin treatment to digest PTDs adsorbed on the cell surface, the PTD-transduced cells were harvested and analysed by flow cytometry. Note that the *y* axis scales for the adherent cell lines are markedly different from that for the nonadherent cell lines. Data shown are the mean ± s.d. of triplicate assays.

membranes (Richard *et al.*, 2003). For this reason, the cells were treated with excess trypsin to eliminate nonspecific plasma membrane binding of the PTDs prior to measurement.

The relative order of their translocation efficiency (Rev > Antp > Tat > VP22), which was based on mean fluorescence, was independent of the cell type (that is, adherent or nonadherent). Furthermore, using PTD-fused Venus, we confirmed that Rev had the highest transduction efficiency (data not shown). Equally important, the overall translocation efficiency of the PTDs depended markedly on whether the cells were adherent (HeLa, HaCaT and A431 cells) or nonadherent (Jurkat, MOLT-4 and HL60 cells). The transduction efficiency was much higher in the adherent cell lines compared with the nonadherent cell lines (Figure 1); note that that the fluorescence (uptake) was about 8- to 25-fold greater in the adherent, than in nonadherent, cell lines.

The cytotoxic properties of the four PTDs were evaluated in adherent (HeLa) and nonadherent (Jurkat) cells. To assess the long-term changes in proliferation, mitochondrial dehydrogenase activity was measured using a WST-8 assay 24 h after PTD treatment. In HeLa cells, there was a remarkable decrease in cell viability when the cells were incubated with Antp at 100 μM, whereas other PTDs were not cytotoxic at the higher concentrations (Figure 2a). In contrast in Jurkat cells, Antp was extremely cytotoxic in a dose-dependent manner and Rev reduced cell proliferation by approximately 40% (Figure 2b). Previous reports indicated that amphipathic peptides, such as transportan, induced cytotoxicity by perturbing the cellular membrane (Hallbrink *et al.*, 2001; Jones *et al.*, 2005; Saar *et al.*, 2005; El-Andaloussi *et al.*, 2007). Thus, the membrane integrity of PTD-treated cells was also measured using an LDH leakage assay. Antp

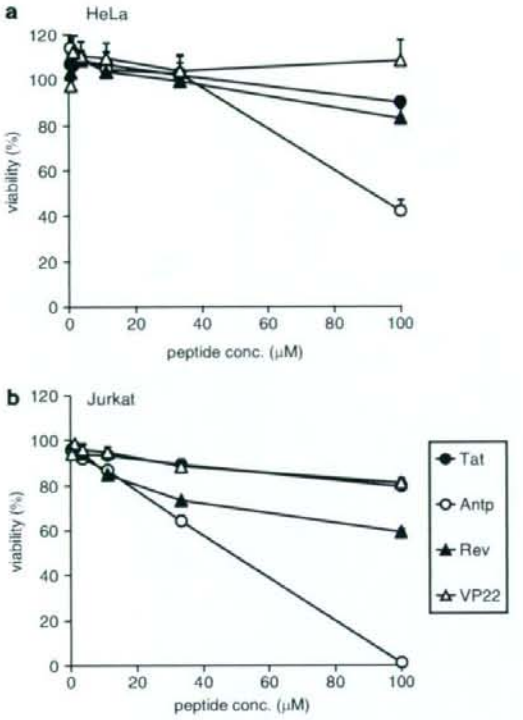


**Figure 2** Viability of protein transduction domain (PTD)-treated cells. HeLa cells (**a**) and Jurkat cells (**b**) were incubated with serially diluted biotin-conjugated Tat, antennapedia (Antp), Rev and VP22 at 37 °C. After 24 h, cell viability was analysed using a WST-8 assay. Data shown are the mean ± s.d. of triplicate assays.

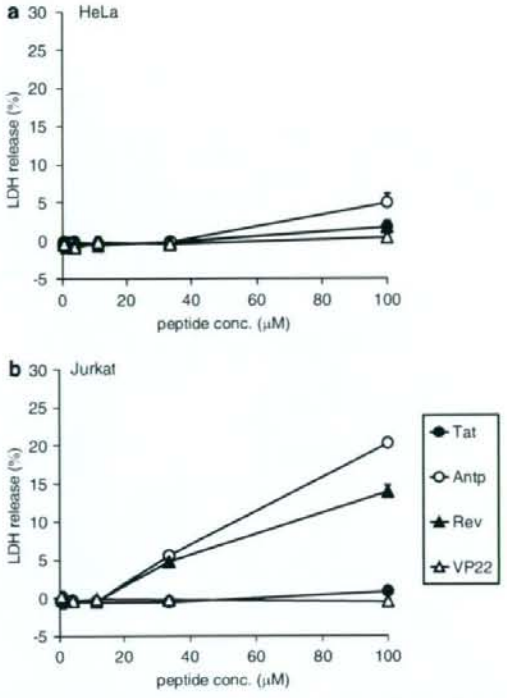


**Figure 3** Membrane integrity of protein transduction domain (PTD)-treated cells. HeLa cells (**a**) and Jurkat cells (**b**) were incubated with serially diluted biotin-conjugated Tat, antennapedia (Antp), Rev and VP22 at 37 °C. After 3 h, the release of lactate dehydrogenase (LDH) was analysed. Data shown are the mean ± s.d. of triplicate assays.

and Rev induced significant LDH leakage in Jurkat cells, but only low LDH leakage was detected in Antp-treated HeLa cells (Figure 3). The membrane-perturbing effect of Antp and Rev contributed to the uptake of peptides, which are shown in Figure 1. Jurkat cells appear more sensitive to Antp or Rev treatment than HeLa cells; this difference in cytotoxicity and translocation efficiency may indicate a difference in the PTD-uptake mode.

*Intracellular transduction mechanism of PTDs*

The results of *in vitro* studies suggest that PTDs enter the cell via an energy-dependent endocytotic pathway (Lundberg *et al.*, 2003; Richard *et al.*, 2003). In particular, studies using various macropinocytosis inhibitors, such as methyl-β-cyclodextrin, to deplete cholesterol from the membrane (Grimmer *et al.*, 2002; Liu *et al.*, 2002), cytochalasin D, to inhibit F-actin elongation (Sampath and Pollard, 1991), or amiloride, to inhibit the $Na^+$-$H^+$ exchanger (West *et al.*, 1989), indicate that Tat is taken up into the cell via lipid raft-dependent macropinocytosis. To the best of our knowledge, however, few comparative studies have analysed the cellular uptake pathway of the four PTDs discussed in this paper. Therefore, we used flow cytometry analysis to determine whether PTD uptake is energy dependent or occurs via lipid raft-mediated macropinocytosis. First, we treated cells with PTD-FAM at 37 or 4 °C and then measured cell fluorescence (Figure 4). At 4 °C, transferrin, which enters cells by clathrin-dependent endocytosis (Schmid, 1997), inhibited the transduction efficiency compared with that at 37 °C. All four PTDs had low transduction ability at 4 °C, indicating that their cellular uptake was energy dependent. We next examined the PTD-FAM uptake efficiency in methyl-β-cyclodextrin-, cytochalasin D- and amiloride-treated HeLa cells. These cell treatments inhibited PTD-FAM incorporation in a dose-dependent manner, but transferrin was not affected (Figure 5). Furthermore, in HeLa cells treated with PTD-FAM, only punctuate fluorescence was observed using confocal laser scanning microscopic analysis (Figure 6). These results indicated that all the PTDs evaluated in this study enter the cell through the macropinocytotic pathway and that most of them were trapped in intracellular vesicles, the macropinosomes.

*Intracellular localization of PTD–protein conjugates*

We next examined the intracellular behaviour of the individual PTDs in more detail. To investigate whether

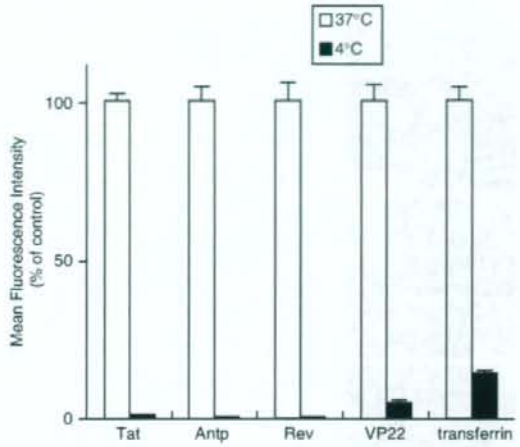


**Figure 4** Effects of temperature on protein transduction domain (PTD) transduction efficiency. HeLa cells were preincubated at 37 or 4 °C for 1 h prior to adding FAM-labelled PTDs or fluorescein isothiocyanate-labelled transferrin for 3 h. Cells were washed in trypsin and analysed by flow cytometry. Data shown are the mean ± s.d. of triplicate assays.

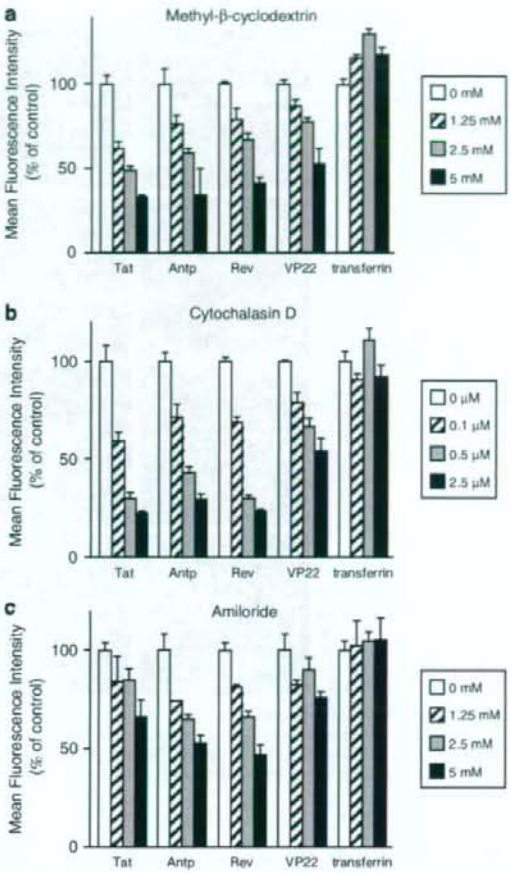


**Figure 5** Effects of endocytosis inhibitors on transduction efficiency of protein transduction domains (PTDs). HeLa cells were pretreated with a range of concentrations of (**a**) methyl-β-cyclodextrin, (**b**) cytochalasin D or (**c**) amiloride for 30 min prior to adding FAM-labelled PTDs or fluorescein isothiocyanate-labelled transferrin for 1 h (**a** and **b**) or 30 min (**c**). Cells were washed in trypsin and analysed by flow cytometry. Data shown are the mean ± s.d. of triplicate assays.

individual PTDs are located in the same vesicles, we used Tat-fused HA2 peptide (HA2-Tat), an influenza virus-derived endosome-disrupting peptide. HA2-Tat improves the activity of Tat-fused Cre recombinase (Wadia *et al.*, 2004). Because HA2 alone cannot enter the cell, HA2-Tat is thought to enter the cell in a Tat-dependent manner and to disrupt the membrane of endosomal vesicles in which the Tat cargo is trapped. Thus, if Antp, Rev and VP22 are trapped in the same vesicles as Tat, the fluorescence should spread throughout the cytosol following cotreatment of the cells with HA2-Tat. As predicted, in HeLa cells cotreated with Antp-, Rev- or VP22-Venus and HA2-Tat, the Venus-derived fluorescence spread throughout the cytosol, whereas in the cells treated with Antp-, Rev- or VP22-Venus alone, only punctuate fluorescence was observed (Figure 7). These results suggested that all the PTDs evaluated in this study entered the cell through a macropinocytotic pathway and were trapped in the same vesicles as Tat.

## Discussion

In the present study, we have systematically compared PTD-mediated molecular transduction mechanisms. Our findings indicated that individual PTDs have different levels of transduction efficiency and cytotoxicity, suggesting that PTDs are internalized into live cells via different mechanisms. We also examined the internalization pathway and intracellular localization of Tat, Antp, Rev and VP22. Unexpectedly, all the PTDs evaluated in this study entered the cell through the macropinocytotic pathway and were trapped in the same vesicles as Tat. The finding that the intracellular transduction pathways of the four PTDs were the same suggests that the method of cell internalization does not contribute to the differences in the PTD transduction efficiency or cytotoxicity. Although the reason for this phenomenon is not clear, we speculate that the primary structure of the individual PTDs or the cell surface proteins that interact with the individual PTDs contribute to the differences in their transduction efficiency and cytotoxicity.

The initial step in the mechanism of cellular entry of PTDs is thought to be the strong ionic interaction between the amino-acid residues of the PTDs and the plasma membrane constituents. Because the translocation is solely physically mediated, the charge distribution and amphipathicity of the peptide and its interaction with the plasma membrane is critical (Pujals *et al.*, 2006). Although most PTDs, if not all, contain a large number of basic amino acids, such as arginine or lysine, the theoretical isoelectric point (pI) value of each PTD used in this study was essentially identical (Tat, Antp,

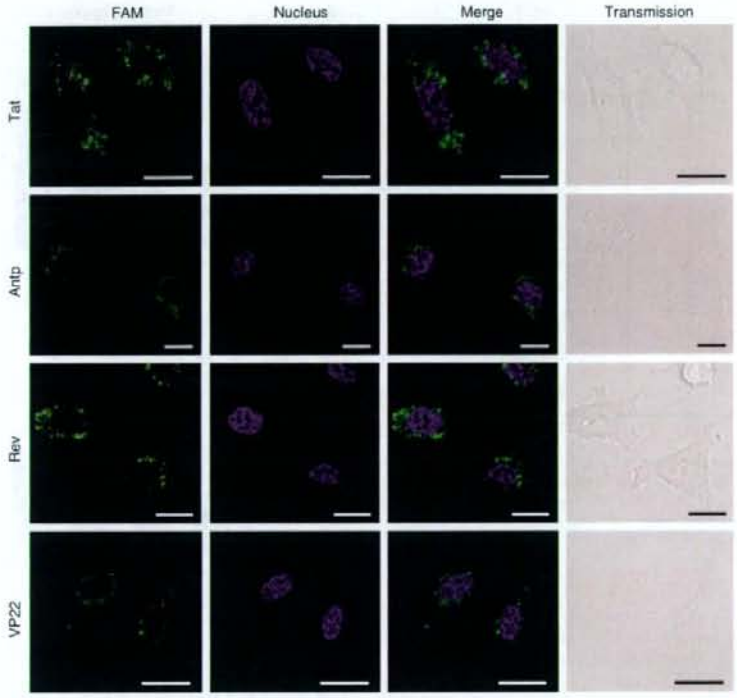


**Figure 6** Intracellular behaviour of protein transduction domain (PTD)-FAM in living cells. HeLa cells were treated with 10 μM PTD-FAM for 3 h. Fluorescence images were acquired using confocal laser scanning microscopy and the signals were merged electronically. The nucleus was counterstained with Hoechst 33342 (blue). From top to bottom: Tat-, antennapedia (Antp)-, Rev- and VP22-FAM. From left to right: FAM (green), nucleus (blue), merged fluorescence and transmission image. Scale bars in each microphotograph indicate 20 μm.

Rev and VP22 have pI values of 12.70, 12.31, 12.60 and 12.01, respectively). Therefore, the internalization efficiency does not appear to depend on the cationic features of the PTDs.

The amphipathicity of the carrier is probably responsible not only for the strong interaction with the lipid membranes (Yandek *et al.*, 2007), but also for the disruption of the cellular membrane, which results in cell death (Hallbrink *et al.*, 2001; Jones *et al.*, 2005; Saar *et al.*, 2005; El-Andaloussi *et al.*, 2007). In terms of cytotoxicity, our data indicate that Antp and Rev both disrupt the membrane (Figure 3), but Rev does not contain an amphipathic structure. Furthermore, there was no correlation between hydrophobicity and transduction efficiency. Thus, differences in the PTD-mediated transduction efficiency and cytotoxicity might be due to the molecular weight or pI of the conjugated cargo.

The cellular events required for internalization, however, differ between reports and are often conflicting. The first mechanistic studies led to the proposal that PTD internalization occurs rapidly in a receptor- and energy-independent manner, perhaps by destabilizing the lipid bilayer or by the formation of inverted micelles with subsequent release of their contents within the intracellular space (Berlose *et al.*, 1996). More recently, an active mechanism based on vesicular uptake was proposed as the general mode of cell internalization of PTDs. In our experiment, although all four PTDs tended to be present in the same vesicles, the detailed mechanism for this colocalization is not yet known. It has been suggested that PTD internalization requires cell surface heparan sulphate proteoglycans (Tyagi *et al.*, 2001; Console *et al.*, 2003; Ziegler and Seelig, 2004). Because Tat interacts electrostatically with heparan sulphate proteoglycan present on the cell surface, it is possible that some PTDs are taken into the same vesicles when they interact with one heparan sulphate proteoglycan. In contrast, as shown in Figure 7, although fluorescence was observed throughout the cytosol, punctate fluorescence was also observed when the cells were cotreated with PTD-Venus and HA2-Tat. This finding suggested that the PTDs did not all exist in the same vesicles and that some PTDs entered the cell through another pathway. This is just speculation, however, and we are now using proteome analysis, such as liquid chromatography coupled with mass spectrometry or two-dimensional gel electrophoresis, to examine whether there are individual cell surface receptors for different PTDs.

In summary, our data suggest that Antp, Rev, VP22 and Tat cross the plasma membrane and reach the macropinosomes via different mechanisms. Our findings also indicate that several issues, such as endosome entrapment and low cell specificity, which limit the therapeutic activity of the cargo,

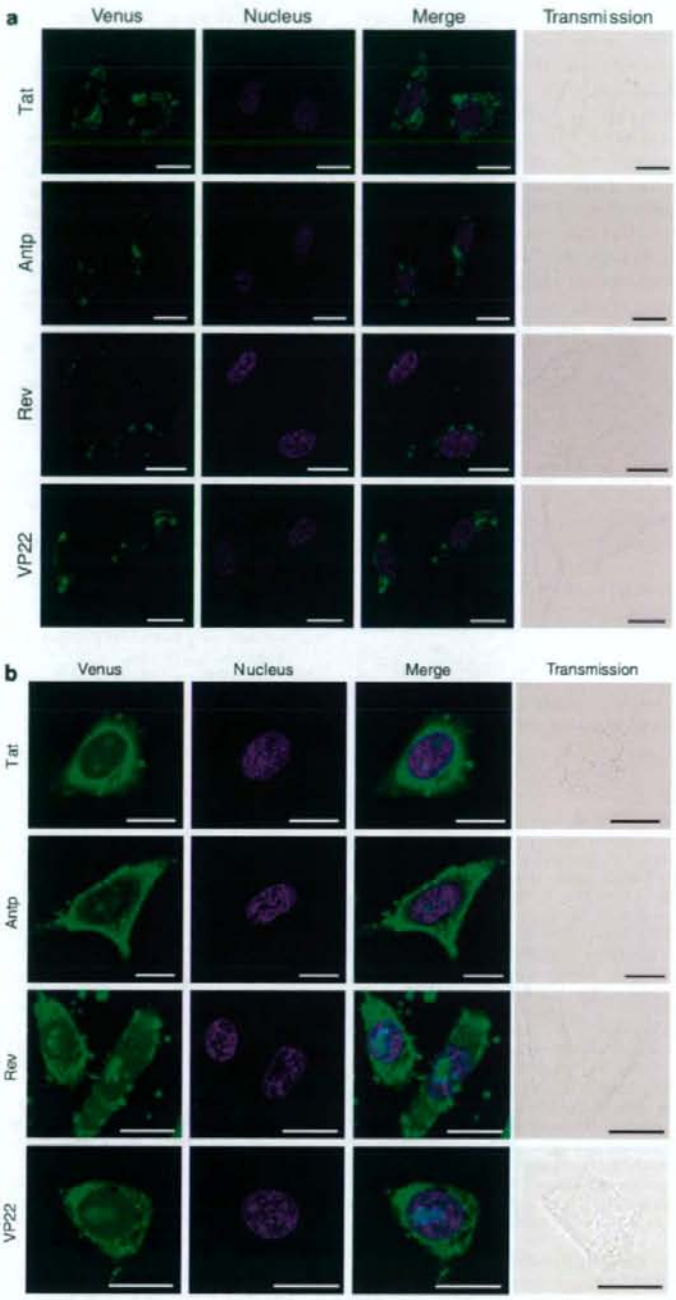


**Figure 7** Intracellular behaviour of protein transduction domain (PTD)-Venus in living cells. HeLa cells were treated with 10 μM PTD-Venus alone (**a**) or 10 μM HA2-Tat (**b**) for 3 h. Fluorescence images were acquired using confocal laser scanning microscopy and the signals were merged electronically. The nucleus was counterstained with Hoechst 33342 (blue). From top to bottom: Tat-, antennapedia (Antp)-, Rev- and VP22-Venus. From left to right: Venus (green), nucleus (blue), merged fluorescence and transmission image. Scale bars in each microphotograph indicate 20 μm.

must be overcome before effective PTD-based drug delivery carriers can be fully developed. We previously reported that cotreatment with HA2-Tat enhances the cytosolic release of Tat-fused peptide-blockers and their biological activities, thereby overcoming the issue of endosome entrapment (Sugita *et al.*, 2007). Furthermore, although the transduction mechanism of PTDs is not yet well understood, these differences led us to explore the possibility of creating novel PTDs. We successfully created novel PTDs that have higher transduction efficiencies than Tat, using a unique phage display-based screening strategy that we previously developed (Mukai *et al.*, 2006; Kamada *et al.*, 2007). Moreover, based on our PTD-screening system, we are currently working to create more useful PTDs with cell type specificity.

## Conflict of interest

The authors state no conflict of interest.

## References

Berlose JP, Convert O, Derossi D, Brunissen A, Chassaing G (1996). Conformational and associative behaviours of the third helix of antennapedia homeodomain in membrane-mimetic environments. *Eur J Biochem* **242**: 372–386.

Borsello T, Forloni G (2007). JNK signalling: a possible target to prevent neurodegeneration. *Curr Pharm Des* **13**: 1875–1886.

Brusic V, Marina O, Wu CJ, Reinherz EL (2007). Proteome informatics for cancer research: from molecules to clinic. *Proteomics* **7**: 976–991.

Chauhan A, Tikoo A, Kapur AK, Singh M (2007). The taming of the cell penetrating domain of the HIV Tat: myths and realities. *J Control Release* **117**: 148–162.

Console S, Marty C, Garcia-Echeverria C, Schwendener R, Ballmer-Hofer K (2003). Antennapedia and HIV transactivator of transcription (TAT) 'protein transduction domains' promote endocytosis of high molecular weight cargo upon binding to cell surface glycosaminoglycans. *J Biol Chem* **278**: 35109–35114.

Derossi D, Joliot AH, Chassaing G, Prochiantz A (1994). The third helix of the Antennapedia homeodomain translocates through biological membranes. *J Biol Chem* **269**: 10444–10450.

Drabik A, Bierczynska-Krzysik A, Bodzon-Kulakowska A, Suder P, Kotlinska J, Silberring J (2007). Proteomics in neurosciences. *Mass Spectrom Rev* **26**: 432–450.

El-Andaloussi S, Jarver P, Johansson HJ, Langel U (2007). Cargo dependent cytotoxicity and delivery efficacy of cell-penetrating peptides: a comparative study. *Biochem J* **407**: 285–292.

Elliott G, O'Hare P (1997). Intercellular trafficking and protein delivery by a herpesvirus structural protein. *Cell* **88**: 223–233.

Ferrari A, Pellegrini V, Arcangeli C, Fittipaldi A, Giacca M, Beltram F (2003). Caveolae-mediated internalization of extracellular HIV-1 tat fusion proteins visualized in real time. *Mol Ther* **8**: 284–294.

Fittipaldi A, Ferrari A, Zoppe M, Arcangeli C, Pellegrini V, Beltram F *et al.* (2003). Cell membrane lipid rafts mediate caveolar endocytosis of HIV-1 Tat fusion proteins. *J Biol Chem* **278**: 34141–34149.

Futaki S, Suzuki T, Ohashi W, Yagami T, Tanaka S, Ueda K *et al.* (2001). Arginine-rich peptides. An abundant source of membrane-permeable peptides having potential as carriers for intracellular protein delivery. *J Biol Chem* **276**: 5836–5840.

Grimmer S, van Deurs B, Sandvig K (2002). Membrane ruffling and macropinocytosis in A431 cells require cholesterol. *J Cell Sci* **115**: 2953–2962.

Hallbrink M, Floren A, Elmquist A, Pooga M, Bartfai T, Langel U (2001). Cargo delivery kinetics of cell-penetrating peptides. *Biochim Biophys Acta* **1515**: 101–109.

Han X, Bushweller JH, Cafiso DS, Tamm LK (2001). Membrane structure and fusion-triggering conformational change of the fusion domain from influenza hemagglutinin. *Nat Struct Biol* **8**: 715–720.

Hawiger J (1999). Noninvasive intracellular delivery of functional peptides and proteins. *Curr Opin Chem Biol* **3**: 89–94.

Joliot A, Prochiantz A (2004). Transduction peptides: from technology to physiology. *Nat Cell Biol* **6**: 189–196.

Jones SW, Christison R, Bundell K, Voyce CJ, Brockbank SM, Newham P *et al.* (2005). Characterisation of cell-penetrating peptide-mediated peptide delivery. *Br J Pharmacol* **145**: 1093–1102.

Kamada H, Okamoto T, Kawamura M, Shibata H, Abe Y, Ohkawa A *et al.* (2007). Creation of novel cell-penetrating peptides for intracellular drug delivery using systematic phage display technology originated from Tat transduction domain. *Biol Pharm Bull* **30**: 218–223.

Kaplan IM, Wadia JS, Dowdy SF (2005). Cationic TAT peptide transduction domain enters cells by macropinocytosis. *J Control Release* **102**: 247–253.

Liu NQ, Lossinsky AS, Popik W, Li X, Gujuluva C, Kriederman B *et al.* (2002). Human immunodeficiency virus type 1 enters brain microvascular endothelia by macropinocytosis dependent on lipid rafts and the mitogen-activated protein kinase signaling pathway. *J Virol* **76**: 6689–6700.

Lundberg M, Wikstrom S, Johansson M (2003). Cell surface adherence and endocytosis of protein transduction domains. *Mol Ther* **8**: 143–150.

Mukai Y, Sugita T, Yamato T, Yamanada N, Shibata H, Imai S *et al.* (2006). Creation of novel protein transduction domain (PTD) mutants by a phage display-based high-throughput screening system. *Biol Pharm Bull* **29**: 1570–1574.

Murriel CL, Dowdy SF (2006). Influence of protein transduction domains on intracellular delivery of macromolecules. *Expert Opin Drug Deliv* **3**: 739–746.

Nagahara H, Vocero-Akbani AM, Snyder EL, Ho A, Latham DG, Lissy NA *et al.* (1998). Transduction of full-length TAT fusion proteins into mammalian cells: TAT-p27Kip1 induces cell migration. *Nat Med* **4**: 1449–1452.

Nori A, Kopecek J (2005). Intracellular targeting of polymer-bound drugs for cancer chemotherapy. *Adv Drug Deliv Rev* **57**: 609–636.

Pujals S, Fernandez-Carneado J, Lopez-Iglesias C, Kogan MJ, Giralt E (2006). Mechanistic aspects of CPP-mediated intracellular drug delivery: relevance of CPP self-assembly. *Biochim Biophys Acta* **1758**: 264–279.

Rhodes DR, Chinnaiyan AM (2005). Integrative analysis of the cancer transcriptome. *Nat Genet* **37** (Suppl): S31–S37.

Richard JP, Melikov K, Brooks H, Prevot P, Lebleu B, Chernomordik LV (2005). Cellular uptake of unconjugated TAT peptide involves clathrin-dependent endocytosis and heparan sulfate receptors. *J Biol Chem* **280**: 15300–15306.

Richard JP, Melikov K, Vives E, Ramos C, Verbeure B, Gait MJ *et al.* (2003). Cell-penetrating peptides. A reevaluation of the mechanism of cellular uptake. *J Biol Chem* **278**: 585–590.

Rojas M, Donahue JP, Tan Z, Lin YZ (1998). Genetic engineering of proteins with cell membrane permeability. *Nat Biotechnol* **16**: 370–375.

Saar K, Lindgren M, Hansen M, Eiriksdottir E, Jiang Y, Rosenthal-Aizman K *et al.* (2005). Cell-penetrating peptides: a comparative membrane toxicity study. *Anal Biochem* **345**: 55–65.

Sampath P, Pollard TD (1991). Effects of cytochalasin, phalloidin, and pH on the elongation of actin filaments. *Biochemistry* **30**: 1973–1980.

Schmid SL (1997). Clathrin-coated vesicle formation and protein sorting: an integrated process. *Annu Rev Biochem* **66**: 511–548.

Schwarze SR, Ho A, Vocero-Akbani A, Dowdy SF (1999). *In vivo* protein transduction: delivery of a biologically active protein into the mouse. *Science* **285**: 1569–1572.

Schwarze SR, Hruska KA, Dowdy SF (2000). Protein transduction: unrestricted delivery into all cells? *Trends Cell Biol* **10**: 290–295.

Skehel JJ, Cross K, Steinhauer D, Wiley DC (2001). Influenza fusion peptides. *Biochem Soc Trans* **29**: 623–626.

Sugita T, Yoshikawa T, Mukai Y, Yamanada N, Imai S, Nagano K *et al.* (2007). Improved cytosolic translocation and tumor-killing